JM PAPERS

Added mass of oscillating bodies in stratified fluids

Bruno Voisin†

Laboratoire des Écoulements Géophysiques et Industriels, Université Grenoble Alpes, CNRS, Grenoble INP, 38000 Grenoble, France

The concept of added mass is generalized to stratified fluids, accounting for the presence of internal waves. Once the added mass of a moving body is known, so is the hydrodynamic force exerted on it by the fluid, and the energy imparted by it to the fluid. As a function of frequency, added mass is complex. Its real part is associated with inertia and its imaginary part, only present in the frequency range of propagating waves, with wave damping. Owing to causality, these two parts satisfy Kramers–Kronig relations. The added masses of an elliptic cylinder of horizontal axis, typical of two-dimensional bodies, and a spheroid of vertical axis, typical of three-dimensional bodies, are deduced from their dipole strengths, themselves deduced from their representations as single layers. The wave power is shown to be a maximum, for fixed oscillation amplitude, at approximately 0.8 times the buoyancy frequency. In the temporal domain, added mass appears as a new memory force taking the form of a convolution integral. The kernel of this integral combines algebraically decaying oscillations at the buoyancy frequency on the one hand; and an exponentially damped oscillation for the horizontal motion of the spheroid, implying short-term memory, an aperiodic algebraic decay for its vertical motion, implying long-term memory, and a constant for the motion of the cylinder, implying everlasting memory, on the other hand. A limitation of the study is its restriction to translational motion.

Key words: internal waves, stratified flows

1. Introduction

A body moving through a fluid experiences an additional inertia, or added mass, imparted to it by the flow that its motion generates within the fluid; see, among others, Kochin, Kibel' & Roze ([1964](#), § 7.7), Batchelor ([1967](#), § 6.4), Lighthill ([1986](#), § 8.3), Landau & Lifshitz ([1987](#), § 11), Saffman ([1992](#), § 5.1) and Newman ([2017](#), §§ 4.12–4.14). The names 'induced' or 'virtual' mass are also used, though the latter is sometimes reserved for

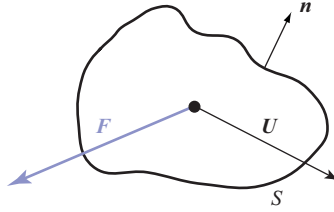† Email address for correspondence: bruno.voisin@cnrs.fr

Figure 1. Dynamics of a rigid body in a homogeneous fluid.

the sum of the actual and added masses (Milne-Thomson 1968, § 9.221; Newman 2017, § 4.16).

Mathematically, added mass is linked to the irrotational dynamics of inviscid fluids. Consider a rigid body of surface S and outward normal n, represented in figure 1, translating at the velocity U without rotation in a fluid of density ρ. A flow of velocity potential ϕ is generated, satisfying the Laplace equation $\nabla^2\phi = 0$ and the free-slip boundary condition $\partial\phi/\partial n = U \cdot n$, with $\partial/\partial n = n \cdot \nabla$ the normal derivative. The linearity of these equations implies a linear relation between U and ϕ. We write $\phi = U_i\phi_i$, where the ϕ_i, with $i = 1, 2, 3$, are functions of x dependent on S and independent of U, satisfying the Laplace equation $\nabla^2\phi_i = 0$ and the boundary condition $\partial\phi_i/\partial n = n_i$; hereinafter the suffix notation is used, and summation over repeated suffixes is implied.

Four quantities are of interest when describing the interaction between the fluid and the body: the impulse I and kinetic energy E of the fluid, given by

$$I = -\rho \int_S n\phi \, \mathrm{d}^2 S, \quad E = -\frac{1}{2}\rho \int_S \phi \frac{\partial\phi}{\partial n} \, \mathrm{d}^2 S, \tag{1.1a,b}$$

and the hydrodynamic force F on the body and the dipole strength $\mathcal{D}$ of this body, given by

$$F = \rho \frac{\mathrm{d}}{\mathrm{d}t} \int_S n\phi \, \mathrm{d}^2 S, \quad \mathcal{D} = \int_S \left(x\frac{\partial\phi}{\partial n} - n\phi \right) \mathrm{d}^2 S, \tag{1.2a,b}$$

with x the position with respect to the body. Defining the symmetric and positive definite added mass tensor as

$$m_{ij} = -\rho \int_S n_i\phi_j \, \mathrm{d}^2 S = -\rho \int_S \frac{\partial\phi_i}{\partial n}\phi_j \, \mathrm{d}^2 S, \tag{1.3}$$

we obtain

$$I_i = m_{ij}U_j, \quad E = \frac{1}{2}m_{ij}U_iU_j, \quad F_i = -m_{ij}\frac{\mathrm{d}U_j}{\mathrm{d}t}, \quad \rho\mathcal{D}_i = (m_f\delta_{ij} + m_{ij})U_j, \tag{1.4a–d}$$

with $m_f = \rho\mathcal{V}$ the mass of the displaced fluid, $\mathcal{V}$ the volume of the body and δ_{ij} the Kronecker delta symbol. Accordingly, added mass characterizes the interaction between the body and the fluid fully.

When, in addition, the fluid supports the propagation of waves, such as acoustic waves (Lighthill 1978, § 1.7) or surface gravity waves (Wehausen 1971; Newman 1978, 2017, §§ 6.15–6.19), added mass becomes complex and varies with the frequency ω. Its real part represents actual inertia and its imaginary part wave damping. Assuming temporal

987 A27-2

variations as $\exp(-\mathrm{i}\omega t)$ and introducing the inertial coefficients $\mu_{ij}(\omega) = \mathrm{Re}\, m_{ij}(\omega)$ and the damping coefficients $\lambda_{ij}(\omega) = \omega\, \mathrm{Im}\, m_{ij}(\omega)$, the oscillations of a body of mass m and position $\boldsymbol{\xi}$ under the influence of an external force $\boldsymbol{F}^e$ satisfy the equation, in suffix notation,

$$[-\omega^2(m\delta_{ij} + \mu_{ij}) - \mathrm{i}\omega\lambda_{ij}]\xi_j = F_i^e. \tag{1.5}$$

Because of causality, the two parts are Hilbert transforms of each other (Roddier 1971, § 13.1; Landau & Lifshitz 1980, § 123). Hence, they satisfy the relations introduced by Kramers and Kronig for the electric permittivity in 1926 and 1927 (Landau & Lifshitz 1984, §§ 77 and 82; Jackson 1999, § 7.10) and applied to added mass by Kotik & Mangulis (1962).

When the body becomes small, viscosity comes into play. Its effect is governed, for a body of size a oscillating in a fluid of kinematic viscosity ν, by the Stokes number $St = \omega a^2/\nu$ representing the ratio of the viscous time scale a^2/ν to the flow time scale $1/\omega$, or the squared ratio of the body size a to the boundary-layer size $(\nu/\omega)^{1/2}$ (Batchelor 1967, § 5.13; Landau & Lifshitz 1987, § 24). Added mass still exists but is accompanied by Stokes resistance and the Basset–Boussinesq force; see Landau & Lifshitz (1987, § 24) for a sphere, and Lawrence & Weinbaum (1986, 1988) and Zhang & Stone (1998) for a spheroid.

Added mass plays an important role in practical applications, ranging from the small scales of particles and bubbles in dispersed two-phase flows (Magnaudet & Eames 2000) to the large scales of floats and ships in naval hydrodynamics (Wehausen 1971; Newman 1978, 2017). Compendia of added masses for a variety of bodies have been given by Brennen (1982), based in part on Kennard (1967), and by Korotkin (2009).

The above is for homogeneous fluids. In the presence of density stratification, buoyancy gives rise to internal waves. Two stratifications have been considered in the literature. The first is uniform, a linear variation of density with depth. Added mass has been determined by Lai & Lee (1981) and Ermanyuk (2002) for a spheroid of vertical axis and Gorgui, Faltas & Ahmed (1995) for a vertical plate, both oscillating. The force and moments on a horizontal elliptic cylinder have been calculated by Hurley (1997) for translational oscillations and Hurley & Hood (2001) for rotational oscillations. The force and moments on a horizontal disc have been calculated by Davis & Llewellyn Smith (2010) and Martin & Llewellyn Smith (2011) for a circular disc and Martin & Llewellyn Smith (2012) for an elliptic disc.

The second stratification is two layer, a homogeneous layer of light fluid atop another layer of heavier fluid. The layers may be semi-infinite, or have finite thicknesses with a rigid bottom and a rigid or free top surface. To determine added mass, multipole expansions have been applied to the oscillations of a horizontal circular cylinder located in either layer (Linton & McIver 1995; Sturova 1999) or intersecting the interface between them (Motygin & Sturova 2002), a sphere located in either layer (Cadby & Linton 2000) and a vertical circular cylinder spanning both layers (You, Shi & Miao 2007). The hybrid element method, combining finite elements around the body and boundary elements away from it, has been applied to a horizontal elliptic cylinder located in the lower layer (Sturova 1994) or intersecting the interface (Sturova 2003; Sturova & Syui 2005). The boundary element method has been applied to a representation of a floating ship known as the Lewis form (Zilman, Kagan & Miloh 1996; Ten & Kashiwagi 2004) and a rectangular box modelling a floating barge (Yeung & Nguyen 1999).

A uniformly stratified layer sandwiched between two homogeneous layers has been considered by Sturova (1999, 2001, 2006) for a horizontal cylinder situated entirely in

the bottom layer, entirely in the middle layer or spanning all three layers, respectively, and a uniformly stratified layer with a rigid bottom and an ice cover by Sturova (2011).

All these studies are theoretical. Experimentally, building on the interpretation of added mass in the time domain as an impulse response function, introduced by Cummins (1962) and Ogilvie (1964) for surface gravity waves, Ermanyuk (2000) developed an original method for measuring added mass in the presence of internal waves, by applying an impulse to the body and deducing the frequency variations of its added mass from the Fourier analysis of the response. This method was applied by Ermanyuk (2000) and Ermanyuk & Gavrilov (2002*b*) to cylinders of circular and diamond-shaped cross-sections, respectively, and Ermanyuk (2002) to oblate and prolate spheroids and a sphere; the oscillations were horizontal, the stratification uniform and the fluid effectively unbounded. The effect of finite depth was investigated by Ermanyuk & Gavrilov (2002*a*) for a circular cylinder, Ermanyuk & Gavrilov (2003) for a sphere and Brouzet *et al.* (2017) for a circular cylinder, a vertical plate and a flat-top hill. A Lewis form in a two-layer fluid was considered by Ten & Kashiwagi (2004).

The present study proposes a general approach of added mass for internal waves in uniform stratification. All the work cited above calculated added mass for specific bodies oscillating in specific directions, except for Ermanyuk (2002) and Ermanyuk & Gavrilov (2002*b*), who presented a general analysis of added mass in the frequency domain, introducing anisotropic coordinate stretching and analytic continuation in frequency so as to relate the added mass of the original body in a stratified fluid to the added mass of the stretched version of the same body in a homogenous fluid. Here, added mass is considered for arbitrary motion of an arbitrary body, both in the time domain and in the frequency domain, and its relation to the various quantities of interest for the dynamics of the body is investigated. Added mass is also related to the boundary integral representation of the body, considered in Voisin (2021). Early versions of smaller scope were presented in summary form by Voisin (2007, 2009). In order to keep the analysis tractable, a number of approximations are made: the fluid is unbounded, uniformly stratified, inviscid, non-diffusive and non-rotating, the Boussinesq approximation is valid, the waves are linear and the body performs translational motion without rotation. The present paper, hereafter referred to as Part 1, investigates the general properties of added mass and discusses two particular cases: the elliptic cylinder of horizontal axis as a typical two-dimensional body, and the spheroid of vertical axis as a typical three-dimensional body. A companion paper (Voisin 2024), the associated Part 2, discusses how past experiments from the literature, involving the oscillation of buoyant bodies about their equilibrium position, may be explained in terms of added mass.

The equations of motion are set in § 2. The hydrostatic response of the fluid is analysed in § 3. For its hydrodynamic response, the modifications to the quantities (1.1)–(1.2) because of the stratification are analysed in § 4, giving two possible definitions of added mass. Consideration of the properties of each leads to the choice of one. The frequency variations of added mass are presented in § 5 for the cylinder and the spheroid, and applied to the wave power, known as a 'conversion rate' within the context of the oceanic internal tide. The temporal aspects of added mass, including the Kramers–Kronig relations, are analysed in § 6. The changes to added mass because of the stratification are interpreted as the addition of a new memory force on the moving body. The main conclusions are summarized in § 7 where their relation to the literature is also discussed.

2. Equations of motion

We are concerned with small disturbances to the state of rest of a stratified fluid where the density distribution $\rho_0(z)$ and the pressure distribution $p_0(z)$ satisfy

$$\frac{\mathrm{d}p_0}{\mathrm{d}z} = -\rho_0 g, \quad \frac{\mathrm{d}\rho_0}{\mathrm{d}z} = -\rho_{00}\frac{N^2}{g}, \tag{2.1a,b}$$

respectively the hydrostatic law and the definition of the buoyancy frequency N, with z the upward vertical coordinate, g the acceleration due to gravity and ρ_{00} a reference density. The stratification is assumed uniform, such that N is a constant, and the Boussinesq approximation is made, according to which the density variations are small and generate buoyancy forces but no inertial forces. The disturbances $\boldsymbol{u} = (u, v, w)$ in velocity, p in pressure and ρ in density satisfy the linearized equations of motion, namely the Euler equation

$$\rho_{00}\frac{\partial \boldsymbol{u}}{\partial t} = -\boldsymbol{\nabla}p - \rho g \boldsymbol{e}_z, \tag{2.2}$$

the equation of continuity

$$\boldsymbol{\nabla} \cdot \boldsymbol{u} = 0 \tag{2.3}$$

and the equation of state

$$\frac{\partial \rho}{\partial t} = \rho_{00}\frac{N^2}{g}w, \tag{2.4}$$

expressing the incompressibility condition $\mathrm{d}(\rho_0 + \rho)/\mathrm{d}t = 0$. Cartesian coordinates (x, y, z) are used, with unit vectors $(\boldsymbol{e}_x, \boldsymbol{e}_y, \boldsymbol{e}_z)$. Time is denoted by t, position by $\boldsymbol{x} = (x, y, z)$ and the del operator by $\boldsymbol{\nabla} = (\partial/\partial x, \partial/\partial y, \partial/\partial z)$.

The equations are solved by introducing the pseudopotential ψ, sometimes called an 'internal potential', in terms of which the fluid dynamical quantities are expressed as

$$\boldsymbol{u} = \left(\frac{\partial^2}{\partial t^2}\boldsymbol{\nabla} + N^2\boldsymbol{\nabla}_h\right)\psi, \quad p = -\rho_{00}\left(\frac{\partial^2}{\partial t^2} + N^2\right)\frac{\partial}{\partial t}\psi, \quad \rho = \rho_{00}\frac{N^2}{g}\frac{\partial^2}{\partial t \partial z}\psi. \tag{2.5a–c}$$

The potential satisfies the wave equation

$$\left(\frac{\partial^2}{\partial t^2}\nabla^2 + N^2\nabla_h^2\right)\psi = 0, \tag{2.6}$$

where $\boldsymbol{\nabla}_h = (\partial/\partial x, \partial/\partial y, 0)$. It was introduced by Sobolev (1954) for inertial waves and Gorodtsov & Teodorovich (1980) for internal waves; see Voisin (1991) for a brief derivation and Voisin (2021) for an updated bibliography.

3. Hydrostatic response

We consider the translation of a rigid body of volume $\mathcal{V}$ and mass m, represented in figure 2, at the velocity $\boldsymbol{U}$. The response of the fluid comprises two parts, one hydrostatic and the other hydrodynamic. We look briefly at the hydrostatic response in this section.
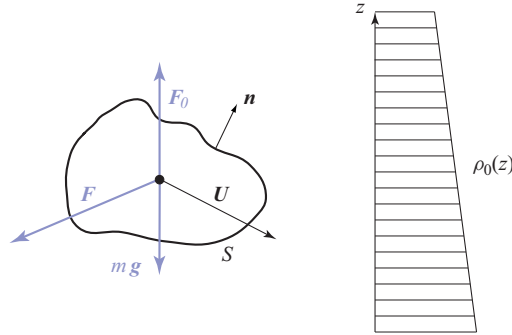
Figure 2. Dynamics of a rigid body in a stratified fluid.

The quantity of interest is the pressure force exerted on the body,

$$F_0 = -\int_S p_0 \boldsymbol{n}\, \mathrm{d}^2 S, \tag{3.1}$$

with S the surface of the body and $\boldsymbol{n}$ its outward normal. Application of Gauss' theorem and use of (2.1a) give

$$F_0 = g\boldsymbol{e}_z \int_V \rho_0(z)\, \mathrm{d}^3 x = m_f g\boldsymbol{e}_z, \tag{3.2}$$

namely Archimedes' force, where V is the region of fluid occupied by the body and $m_f = \int_V \rho_0(z)\, \mathrm{d}^3 x$ is the mass of the displaced fluid.

We set $z = 0$ at the level where the body is neutrally buoyant, namely where its weight balances Archimedes' force, and we introduce the position ζ of its centroid with respect to this level, such that $\mathcal{V}\zeta = \int_V z\, \mathrm{d}^3 x$. Writing, by (2.1$b$),

$$\rho_0(z) = \rho_0(0)\left(1 - \frac{N^2}{g}z\right), \tag{3.3}$$

we obtain $m = \rho_0(0)\mathcal{V}$ and

$$F_0 = mg\boldsymbol{e}_z - mN^2\zeta\boldsymbol{e}_z. \tag{3.4}$$

Similar derivations may be found in Larsen (1969) and Lai & Lee (1981).

4. Hydrodynamic response

The hydrodynamic response is due to the free-slip forcing at S, namely, using (2.5a),

$$\left(\frac{\partial^2}{\partial t^2}\frac{\partial}{\partial n} + N^2\frac{\partial}{\partial n_h}\right)\psi = \boldsymbol{n}\cdot\boldsymbol{U} \quad (\boldsymbol{x} \in S), \tag{4.1}$$

where $\partial/\partial n = \boldsymbol{n}\cdot\boldsymbol{\nabla}$ and $\partial/\partial n_h = \boldsymbol{n}\cdot\boldsymbol{\nabla}_h$. With S a moving surface, this forcing is not linear. For it to become so, an assumption of a small displacement of the body compared with its size must be introduced, allowing S to be considered fixed.

Stokes (1851, §41), however, pointed out that this assumption may be relaxed. For the flow of a homogeneous viscous fluid, at small velocities $\boldsymbol{U}$ of the body and $\boldsymbol{u}$ of the fluid, he noted that the switch to a system of coordinates moving with the body leaves the linear equations of motion unchanged – since the convective terms associated with the switch are

987 A27-6

of second order in the small velocities – and makes S fixed. Gatignol (1983) and Maxey & Riley (1983) implemented the switch analytically. The boundary condition becomes linear, without requiring small displacements. The results may thus be applied to a body moving along an arbitrary path.

The same is true here: with $\boldsymbol{\xi}(t)$ the position of the body and $\boldsymbol{U}(t) = \mathrm{d}\boldsymbol{\xi}/\mathrm{d}t$ its velocity, assumed small, a switch to the coordinates $\boldsymbol{x}' = \boldsymbol{x} - \boldsymbol{\xi}(t)$ and $t' = t$ gives

$$\boldsymbol{\nabla} = \boldsymbol{\nabla}', \quad \frac{\partial}{\partial t} = \frac{\partial}{\partial t'} - \boldsymbol{U} \cdot \boldsymbol{\nabla}', \tag{4.2}$$

yielding additional terms $\rho_{00}\boldsymbol{U} \cdot \boldsymbol{\nabla}'\boldsymbol{u}$ in (2.2) and $\boldsymbol{U} \cdot \boldsymbol{\nabla}'\rho$ in (2.4), both negligible. In the following we omit the primes and take (2.2)–(2.4) as our equations of motion and (4.1) as our boundary condition, on the understanding that S is fixed. This will allow the application of the results to a body moving along an arbitrary path in § 6.2.

Now, the linearity of (2.6) and (4.1) implies a linear relation between the forcing $\boldsymbol{U}(t)$ and its effect $\psi(\boldsymbol{x}, t)$. The most general such relation is a temporal convolution (Landau & Lifshitz 1980, § 123, 1984, § 77; Jackson 1999, § 7.10) of the form

$$\psi(\boldsymbol{x}, t) = U_i(t) * \psi_i(\boldsymbol{x}, t) = \int U_i(t')\psi_i(\boldsymbol{x}, t - t') \, \mathrm{d}t', \tag{4.3}$$

with $*$ the convolution operator. Hereinafter the suffix notation is used, with i ranging over 1, 2 and the vertical direction 3, and summation over repeated suffixes is implied. The ψ_i are functions of $\boldsymbol{x}$ and t dependent on S and independent of $\boldsymbol{U}$. They satisfy the wave equation

$$\left(\frac{\partial^2}{\partial t^2}\nabla^2 + N^2\nabla_h^2\right)\psi_i = 0, \tag{4.4}$$

and the boundary condition

$$\left(\frac{\partial^2}{\partial t^2}\frac{\partial}{\partial n} + N^2\frac{\partial}{\partial n_h}\right)\psi_i = n_i\delta(t) \quad (\boldsymbol{x} \in S), \tag{4.5}$$

with $\delta(t)$ the Dirac delta function. They represent the internal potential due to a unit velocity impulse $U_i(t) = \delta(t)$ along the x_i direction, or a unit step displacement $\xi_i(t) = H(t)$ with $H(t)$ the Heaviside step function.

We investigate now the four quantities involved in the definition of added mass, discussed in § 1, for convenience in a different order.

4.1. *Hydrodynamic force*

The hydrodynamic force on the body is

$$\boldsymbol{F}(t) = -\int_S p\boldsymbol{n} \, \mathrm{d}^2 S, \tag{4.6}$$

namely, by (2.5),

$$\boldsymbol{F}(t) = \rho_{00}\frac{\mathrm{d}}{\mathrm{d}t}\int_S \boldsymbol{n}\left(\frac{\partial^2}{\partial t^2} + N^2\right)\psi \, \mathrm{d}^2 S. \tag{4.7}$$

Use of (4.3) yields

$$F_i(t) = -m_{ij}(t) * \frac{\mathrm{d}U_j}{\mathrm{d}t}, \tag{4.8}$$

where

$$m_{ij}(t) = -\rho_{00} \int_S n_i \left(\frac{\partial^2}{\partial t^2} + N^2 \right) \psi_j \, d^2 S, \tag{4.9}$$

or equivalently

$$m_{ij}(t) = -\rho_{00} \left(\frac{d^2}{dt^2} + N^2 \right) \int_S n_i \psi_j \, d^2 S, \tag{4.10}$$

constitutes a first possible definition of added mass, introduced by Ermanyuk (2002) and Ermanyuk & Gavrilov (2002b) in monochromatic form.

4.2. *Wave energy*

The scalar product of u with (2.2), combined with (2.3) and (2.4), provides the energy conservation equation

$$\frac{\partial}{\partial t} \left(\frac{1}{2} \rho_{00} u^2 + \frac{1}{2} \frac{g^2}{N^2} \frac{\rho^2}{\rho_{00}} \right) + \nabla \cdot (p u) = 0. \tag{4.11}$$

Accordingly, $\rho_{00} u^2/2 + g^2 \rho^2 / 2\rho_{00} N^2$ is the wave energy density, combining kinetic and potential energy, and $p u$ the wave energy flux, namely a vector whose scalar product with n represents the rate at which energy is transported across a unit surface element of normal n.

The total power output of the body follows from integrating this flux over S, to give

$$P = \int_S p u \cdot n \, d^2 S = -U \cdot F, \tag{4.12}$$

that is,

$$P(t) = U_i(t) \left[m_{ij}(t) * \frac{dU_j}{dt} \right]. \tag{4.13}$$

The same added mass tensor is involved as for the hydrodynamic force, consistent with the fact that the energy of the fluid varies in response to the work of the hydrodynamic force $-F$ exerted by the body on the fluid.

4.3. *Wave momentum*

Momentum conservation is written in flux form, by (2.2) and (2.5), as

$$\frac{\partial}{\partial t} (\rho_{00} u_i) + \frac{\partial \Pi_{ij}}{\partial x_j} = 0, \tag{4.14}$$

where

$$\Pi_{ij} = p \delta_{ij} + \rho_{00} N^2 \delta_{i3} \delta_{j3} \frac{\partial \psi}{\partial t} = -\rho_{00} \left[\delta_{ij} \frac{\partial^2}{\partial t^2} + (\delta_{i1}\delta_{j1} + \delta_{i2}\delta_{j2}) N^2 \right] \frac{\partial \psi}{\partial t}, \tag{4.15}$$

with δ_{ij} the Kronecker delta symbol, is the wave momentum flux, namely a tensor whose contraction with n represents the rate at which momentum is transported across a unit surface element of normal n.

The total momentum output of the body follows as

$$\boldsymbol{I} = -\rho_{00} \int_S \left(\boldsymbol{n} \frac{\partial^2}{\partial t^2} + \boldsymbol{n}_h N^2 \right) \psi \, \mathrm{d}^2 S, \tag{4.16}$$

with $\boldsymbol{n}_h$ the horizontal projection of $\boldsymbol{n}$, namely

$$I_i(t) = m'_{ij}(t) * U_j(t), \tag{4.17}$$

where

$$m'_{ij}(t) = -\rho_{00} \int_S \left[n_i \frac{\partial^2}{\partial t^2} + (n_1 \delta_{i1} + n_2 \delta_{i2}) N^2 \right] \psi_j \, \mathrm{d}^2 S, \tag{4.18}$$

or equivalently

$$m'_{ij}(t) = -\rho_{00} \left(\frac{\mathrm{d}^2}{\mathrm{d} t^2} + N^2 \right) \int_S n_i \psi_j \, \mathrm{d}^2 S \quad (i = 1, 2), \tag{4.19a}$$

$$m'_{3j}(t) = -\rho_{00} \frac{\mathrm{d}^2}{\mathrm{d} t^2} \int_S n_3 \psi_j \, \mathrm{d}^2 S, \tag{4.19b}$$

constitutes a second possible definition of added mass. Consistent with (4.15), the difference between the two definitions follows from the fact that not only pressure but also buoyancy contribute to changing the momentum of the fluid.

4.4. *Dipole strength*

The dipole strength of the body may be derived from a Kirchhoff–Helmholtz integral, by expanding this integral at large distances from the body; see Batchelor (1967, §§ 2.9 and 6.4) and Lighthill (1986, §§ 8.1–8.3) for fluid flow, and Pierce (2019, § 4.6) for acoustic waves. The integral and its expansion are obtained for internal waves in Appendix B, using the Green's function introduced in Appendix A. Arbitrary forcing within a surface S of outward normal $\boldsymbol{n}$, generating the internal potential ψ and the normal velocity $u_n = \boldsymbol{n} \cdot \boldsymbol{u}$ at the surface, has the monopole strength

$$\mathcal{S}(t) = \int_S u_n(\boldsymbol{x}, t) \, \mathrm{d}^2 S, \tag{4.20}$$

and the dipole strength

$$\boldsymbol{\mathcal{D}}(t) = \int_S \left[\boldsymbol{x} u_n(\boldsymbol{x}, t) - \left(\boldsymbol{n} \frac{\partial^2}{\partial t^2} + \boldsymbol{n}_h N^2 \right) \psi(\boldsymbol{x}, t) \right] \mathrm{d}^2 S. \tag{4.21}$$

For a rigid body, we have $\int_S n_i \, \mathrm{d}^2 S = 0$ and $\int_S x_i n_j \, \mathrm{d}^2 S = \mathcal{V} \delta_{ij}$. Accordingly,

$$\mathcal{S} = 0, \quad \rho_{00} \boldsymbol{\mathcal{D}} = \boldsymbol{I} + m_f U, \tag{4.22a,b}$$

with $m_f = \rho_{00} \mathcal{V}$ the mass of the displaced fluid, so that

$$\rho_{00} \mathcal{D}_i(t) = [m_f \delta_{ij} \delta(t) + m'_{ij}(t)] * U_j(t), \tag{4.23}$$

an expression of the dipole strength involving the same added mass tensor as for the wave momentum.

4.5. *Symmetry*

In order to decide which definition of added mass is the most relevant – m_{ij} given by (4.9)–(4.10) or m'_{ij} given by (4.18)–(4.19) – we start by looking at their symmetry. The Green's theorem (B2) is applied to the volume delimited by the surface S of the body and a sphere S_R of large radius R, and to the time range $]-\infty, +\infty[$. The functions are chosen as ψ_i and ψ_j. These are zero at $t = -\infty$, and their temporal derivatives vanish as $t \to +\infty$, consistent with the behaviours exhibited later in § 6.2 for the impulse response functions. Accordingly, the initial and final contributions vanish. The body, being rigid, acts as a dipole, so that ψ_i and ψ_j decrease as $1/R^2$ and their gradients as $1/R^3$. The contribution of S_R vanishes, and we obtain

$$\int dt \int_V d^3x \left[\psi_i \left(\frac{\partial^2}{\partial t^2} \nabla^2 + N^2 \nabla_h^2 \right) \psi_j - \psi_j \left(\frac{\partial^2}{\partial t^2} \nabla^2 + N^2 \nabla_h^2 \right) \psi_i \right]$$
$$= -\int dt \int_S d^2S \left[\psi_i \left(\frac{\partial^2}{\partial t^2} \frac{\partial}{\partial n} + N^2 \frac{\partial}{\partial n_h} \right) \psi_j - \psi_j \left(\frac{\partial^2}{\partial t^2} \frac{\partial}{\partial n} + N^2 \frac{\partial}{\partial n_h} \right) \psi_i \right], \quad (4.24)$$

namely, by (4.4) and (4.5),

$$\int_S n_i \psi_j \, d^2S = \int_S n_j \psi_i \, d^2S. \quad (4.25)$$

We thus have

$$m_{ij} = m_{ji}, \quad m'_{ij} \neq m'_{ji}, \quad (4.26a,b)$$

implying that the first definition of added mass is symmetric while the second is not. This provides a first hint that m_{ij} may be the best choice.

4.6. *Monochromatic case*

Now, the situations investigated in practice are often monochromatic, either because the forcing is of this type, or because temporal Fourier transforms are used. We define direct and inverse transforms according to

$$f(\omega) = \int f(t) \exp(i\omega t) \, dt, \quad f(t) = \frac{1}{2\pi} \int f(\omega) \exp(-i\omega t) \, d\omega. \quad (4.27a,b)$$

The added masses (4.9) and (4.18) have the transforms

$$m_{ij}(\omega) = \rho_{00}(\omega^2 - N^2) \int_S n_i \psi_j(\boldsymbol{x}, \omega) \, d^2S, \quad (4.28)$$

$$m'_{ij}(\omega) = \rho_{00} \int_S [\omega^2 n_i - N^2(n_1 \delta_{i1} + n_2 \delta_{i2})] \psi_j(\boldsymbol{x}, \omega) \, d^2S, \quad (4.29)$$

respectively, and are related to each other by

$$m_{ij}(\omega) = m'_{ij}(\omega) \quad (i = 1, 2), \qquad m_{3j}(\omega) = \left(1 - \frac{N^2}{\omega^2} \right) m'_{3j}(\omega). \quad (4.30a,b)$$

We consider waves of frequency ω, varying with time through the factor $\exp(-i\omega t)$ that is suppressed in the following. For this, the body is assumed to oscillate at the velocity $\boldsymbol{U} \exp(-i\omega t)$, where the instant $t = 0$ is chosen such that the components U_i of $\boldsymbol{U}$ are real and positive. The linear fluid dynamical quantities become

987 A27-10

$$F_i = \mathrm{i}\omega m_{ij}(\omega)U_j, \quad I_i = m'_{ij}(\omega)U_j, \quad \rho_{00}\mathcal{D}_i = [m_f\delta_{ij} + m'_{ij}(\omega)]U_j, \quad (4.31a\text{–}c)$$

and have zero phase average. Wave power is a quadratic quantity. Decomposing the tensor $m_{ij}(\omega)$ into an inertial part $\mu_{ij}(\omega)$ and a wave damping part $\lambda_{ij}(\omega)$, such that

$$\mu_{ij}(\omega) = \mathrm{Re}\, m_{ij}(\omega), \quad \lambda_{ij}(\omega) = \omega\,\mathrm{Im}\, m_{ij}(\omega), \quad (4.32a,b)$$

and using the result that the product of two quantities of complex amplitudes A and B has the phase average $\mathrm{Re}[A\bar{B}]/2$, where the overbar denotes a complex conjugate, the average wave power follows as

$$\langle P \rangle = \frac{1}{2}\lambda_{ij}(\omega)U_iU_j. \quad (4.33)$$

This quadratic form, representing energy dissipation, is necessarily positive definite, implying that the tensor $\lambda_{ij}(\omega)$ is also positive definite.

4.7. *Which added mass?*

The first definition of added mass, m_{ij}, thus appears as the most relevant. It is symmetric while the second definition, m'_{ij}, is not. The two quantities expressed in terms of it – the hydrodynamic force and the wave energy – are the most interesting in practice. By contrast, the two quantities expressed in terms of m'_{ij} are of meagre interest: the wave momentum has zero phase average, and one must switch to the pseudomomentum to get actual momentum transport (Bühler 2014); monochromatic waves propagate in beams along which, whatever the distance, the wave profile still depends on the details of the forcing, not on its dipole strength alone (Lighthill 1978, § 4.10; Voisin 2003).

In the following we define added mass as m_{ij}, but still use m'_{ij} to determine it. Specifically, the boundary integral method (Voisin 2021) provides a representation of an oscillating body as a source term $q(x)$ in the wave equation (2.6), and from it the dipole strength

$$\mathcal{D} = \int x q(x)\, \mathrm{d}^3x. \quad (4.34)$$

Once this strength is known, so is $m'_{ij}(\omega)$ by (4.31c), then $m_{ij}(\omega)$ by (4.30).

5. Frequency-dependent aspects

5.1. *Added mass*

We consider now the added mass coefficients

$$C_{ij}(\omega) = \frac{m_{ij}(\omega)}{m_f} \quad (5.1)$$

of typical oscillating bodies: an elliptic cylinder of horizontal axis in two dimensions, and a spheroid of vertical axis in three dimensions. Single-layer representations $q(x)$ of these bodies were given in table 5 of Voisin (2021), along with their spectra $q(k)$. Expanding these at small wavenumber, as

$$q(k) = \int q(x)\exp(-\mathrm{i}k\cdot x)\,\mathrm{d}^3x \sim -\mathrm{i}k\cdot\mathcal{D}, \quad (5.2)$$

provides immediately the dipole strengths $\mathcal{D}$ and from them the added masses.

The cylinder is assumed to have horizontal y axis and semi-axes a and b in the vertical (x, z) plane, respectively, and to oscillate at the velocity $(U, 0, W) \exp(-\mathrm{i}\omega t)$. We obtain, per unit length along the y direction,

$$\mathcal{D}_x = \pi ab(1 + \varUpsilon)U, \quad \mathcal{D}_y = 0, \quad \mathcal{D}_z = \pi ab \left(1 + \frac{1}{\varUpsilon}\right) W, \tag{5.3a–c}$$

where

$$\varUpsilon = \epsilon \left(1 - \frac{1}{\varOmega^2}\right)^{1/2}, \tag{5.4}$$

with $\epsilon = b/a$ the aspect ratio and $\varOmega = \omega/N$ the frequency ratio. The added mass coefficients are given in table 1 for the elliptic cylinder and its particular cases: the circular cylinder ($\epsilon = 1$), the horizontal plate ($\epsilon = 0$) and the vertical plate ($\epsilon = \infty$). The coordinates axes are principal axes and the added mass tensor is diagonal, leading to the simplified notations $C_x = C_{11}$ and $C_z = C_{33}$.

Consistent with causality, the coefficients are analytic functions in the upper half of the complex $\varOmega$ plane. The branch cuts emanating from the branch points $\varOmega = \pm 1$ are taken vertically downwards, yielding

$$\varUpsilon = |\varUpsilon| \quad (|\varOmega| > 1), \quad \mathrm{i}|\varUpsilon| \operatorname{sign} \varOmega \quad (|\varOmega| < 1) \tag{5.5a,b}$$

along the real $\varOmega$ axis.

For the spheroid, of vertical z axis and semi-axes a and b along the horizontal and the vertical, respectively, oscillating at the same velocity, the dipole strength is

$$\mathcal{D}_x = \frac{4}{3}\pi a^2 b \frac{2U}{1 + D(\varUpsilon)}, \quad \mathcal{D}_y = 0, \quad \mathcal{D}_z = \frac{4}{3}\pi a^2 b \frac{W}{1 - D(\varUpsilon)}, \tag{5.6a–c}$$

where

$$D(\varUpsilon) = \frac{1}{1 - \varUpsilon^2} \left[1 - \varUpsilon \frac{\arccos \varUpsilon}{(1 - \varUpsilon^2)^{1/2}}\right], \tag{5.7}$$

becoming

$$D(\varUpsilon) = \frac{1}{1 - |\varUpsilon|^2} \left[1 - |\varUpsilon| \frac{\arccos |\varUpsilon|}{(1 - |\varUpsilon|^2)^{1/2}}\right] \quad (|\varOmega| > 1 \text{ and } |\varUpsilon| < 1) \tag{5.8a}$$

$$= \frac{1}{1 - |\varUpsilon|^2} \left[1 - |\varUpsilon| \frac{\operatorname{arccosh} |\varUpsilon|}{(|\varUpsilon|^2 - 1)^{1/2}}\right] \quad (|\varOmega| > 1 \text{ and } |\varUpsilon| > 1) \tag{5.8b}$$

$$= \frac{1}{1 + |\varUpsilon|^2} \left[1 - |\varUpsilon| \frac{\operatorname{arcsinh} |\varUpsilon| + \mathrm{i}(\pi/2) \operatorname{sign} \varOmega}{(1 + |\varUpsilon|^2)^{1/2}}\right] \quad (|\varOmega| < 1) \tag{5.8c}$$

along the real $\varOmega$ axis. The added mass coefficients are given in table 1 for the spheroid and its particular cases: the sphere ($\epsilon = 1$), the horizontal disc ($\epsilon = 0$) and the vertical needle ($\epsilon = \infty$).

The particular results from the literature are all recovered. As $\varOmega \to \infty$, the inertial coefficients of the cylinder and the spheroid in a homogeneous fluid are also recovered.

987 A27-12

Oscillating body	Horizontal motion	Vertical motion	Comments
Elliptic cylinder	$C_x(\omega) = \epsilon \left(1 - \dfrac{1}{\Omega^2}\right)^{1/2}$	$C_z(\omega) = \dfrac{1}{\epsilon}\left(1 - \dfrac{1}{\Omega^2}\right)^{1/2}$	$C_x^\infty = \epsilon, \quad C_z^\infty = \dfrac{1}{\epsilon}$
Circular cylinder	$C_x(\omega) = \left(1 - \dfrac{1}{\Omega^2}\right)^{1/2}$	$C_z(\omega) = \left(1 - \dfrac{1}{\Omega^2}\right)^{1/2}$	$C_x^\infty = C_z^\infty = 1$
Horizontal plate	$C_x(\omega) = 0$	$C_z(\omega) = \infty$	$m_x(\omega) = 0, \quad m_z(\omega) = \pi\rho_{00}a^2\left(1 - \dfrac{1}{\Omega^2}\right)^{1/2}, \quad m_z(\omega) = 0$
Vertical plate	$C_x(\omega) = \infty$	$C_z(\omega) = 0$	$m_x(\omega) = \pi\rho_{00}b^2\left(1 - \dfrac{1}{\Omega^2}\right)^{1/2}$
Spheroid	$C_x(\omega) = \dfrac{1 - D(\Upsilon)}{1 + D(\Upsilon)}$	$C_z(\omega) = \left(1 - \dfrac{1}{\Omega^2}\right)\dfrac{D(\Upsilon)}{1 - D(\Upsilon)}$	$C_x^\infty = \dfrac{1 - D(\epsilon)}{1 + D(\epsilon)}, \quad C_z^\infty = \dfrac{D(\epsilon)}{1 - D(\epsilon)}$
Sphere	$C_x(\omega) = \dfrac{1 - D(\Upsilon)}{1 + D(\Upsilon)}$	$C_z(\omega) = \left(1 - \dfrac{1}{\Omega^2}\right)\dfrac{D(\Upsilon)}{1 - D(\Upsilon)}$	$C_x^\infty = C_z^\infty = \dfrac{1}{2}$
Horizontal disc	$C_x(\omega) = 0$	$C_z(\omega) = \infty$	$m_x(\omega) = 0, \quad m_z(\omega) = \dfrac{8}{3}\rho_{00}a^3\left(1 - \dfrac{1}{\Omega^2}\right)^{1/2}$
Vertical needle	$C_x(\omega) = \infty$	$C_z(\omega) = 0$	$m_x(\omega) = m_z(\omega) = 0$

Table 1. Added mass coefficients for the elliptic cylinder and the spheroid, together with their values for aspects ratios $\epsilon = 0$, 1 and ∞ and their limit for frequency ratio $\Omega \to \infty$. The quantities Υ and $D(\Upsilon)$ are defined in (5.4) and (5.7), respectively.
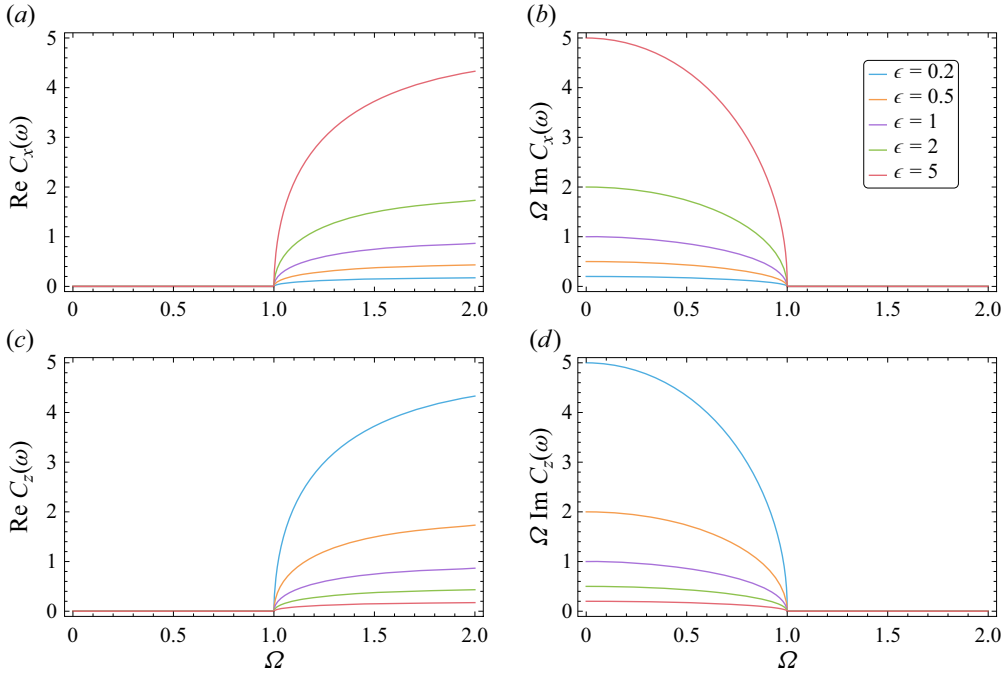
Figure 3. Frequency variations of (*a*,*c*) the inertial coefficients Re $C_x(\omega)$ and Re $C_z(\omega)$ and (*b*,*d*) the damping coefficients Ω Im $C_x(\omega)$ and Ω Im $C_z(\omega)$ of an elliptic cylinder of aspect ratio ϵ oscillating (*a*,*b*) horizontally or (*c*,*d*) vertically.

They are denoted as C_x^∞ and C_z^∞ and involve

$$D(\epsilon) = \frac{1}{1-\epsilon^2}\left[1 - \epsilon\frac{\arccos\epsilon}{(1-\epsilon^2)^{1/2}}\right] \quad (\epsilon < 1) \qquad (5.9a)$$

$$= \frac{1}{1-\epsilon^2}\left[1 - \epsilon\frac{\text{arccosh}\,\epsilon}{(\epsilon^2-1)^{1/2}}\right] \quad (\epsilon > 1) \qquad (5.9b)$$

for the spheroid, becoming $D(1) = 1/3$ for the sphere.

The frequency variations of added mass are plotted in figures 3 and 4. They are consistent with the measurements by Ermanyuk (2000), Ermanyuk & Gavrilov (2002*a*) and Brouzet *et al.* (2017) for a circular cylinder, Ermanyuk (2002) and Ermanyuk & Gavrilov (2003) for a sphere and Ermanyuk (2002) for oblate and prolate spheroids, all for horizontal oscillations. Wave damping is only observed in the frequency range $|\Omega| < 1$ of propagating waves, and vanishes at $|\Omega| > 1$ for evanescent waves. For the cylinder, there is no inertial added mass in the propagating case, but the same is not true for the spheroid. The damping coefficient does not vanish at zero frequency for the cylinder, while the inertial coefficient diverges logarithmically for the vertical motion of the spheroid. These remarks will have implications when formulating the Kramers–Kronig relations in § 6.1.

5.2. *Energy radiation*

An important manifestation of internal waves in the ocean is the so-called internal or baroclinic tide, generated by the ebb and flow of the barotropic tide over bottom topography (Garrett & Kunze 2007) or at the continental slope (Baines 1982). Together
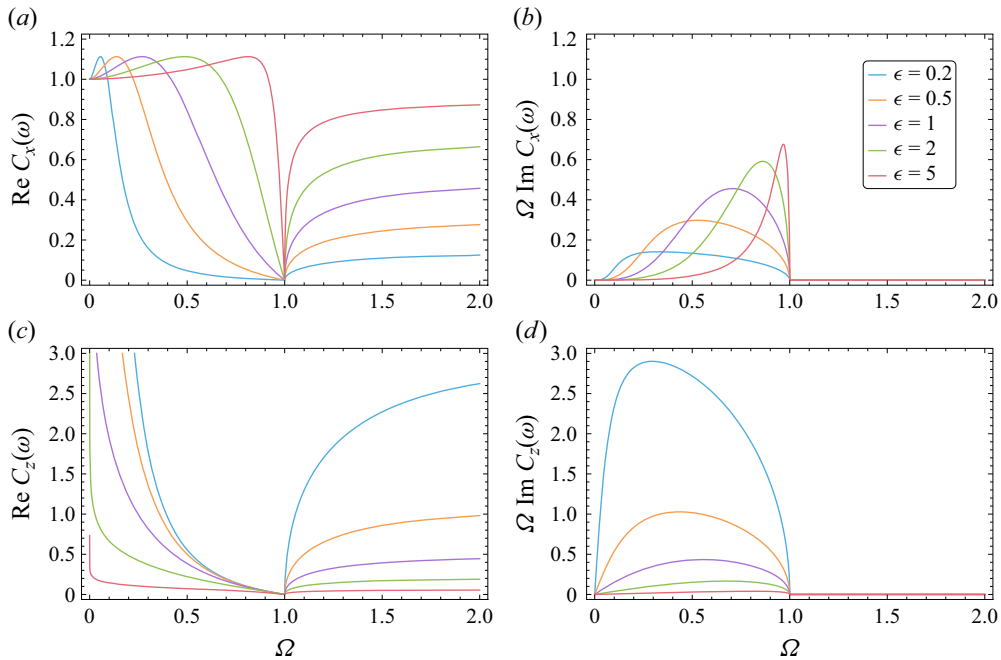
987 A27-14

Figure 4. Same as figure 3 for a spheroid.

with wind-generated waves at the surface, and lee waves generated by the flow of ocean currents over bottom topography, the internal tide is now thought to play an essential part in the mixing of the ocean (Ferrari & Wunsch 2009; Ferrari 2014; Ferrari *et al.* 2016; MacKinnon *et al.* 2017; Sarkar & Scotti 2017; Whalen *et al.* 2020; Legg 2021). For small tidal excursion, namely small amplitude of the barotropic tidal motion compared with the width of the topography, the problem is linear and equivalent to the oscillation of the topography in an ocean at rest. In this context, the average wave power $\langle P \rangle$ represents the rate at which barotropic energy is converted to baroclinic form; hence, the name, sometimes used, of 'conversion rate' (Llewellyn Smith & Young 2002). For a recent study of its calculation in a general setting and an up-to-date bibliography, see Papoutsellis, Mercier & Grisouard (2023).

Topographies are called subcritical or supercritical depending on whether their maximum slope is smaller or larger than the slope of the wave rays, respectively, inclined at the angle arcsin Ω to the horizontal. The waves radiated by supercritical topography take the form of critical beams tangential to the topography; these are thinner than the beams from subcritical topography, hence, are more prone to breaking and mixing. See Machicoane *et al.* (2015) and Le Dizès & Le Bars (2017) for discussions of critical beams in the context of inertial waves. The semi-elliptic ridge and the hemispheroidal seamount, which are the oceanic analogues of the elliptic cylinder and the spheroid, are unconditionally supercritical, irrespective of the tidal frequency. Their experimental or numerical studies include Zhang, King & Swinney (2007) for a semi-circular ridge, King, Zhang & Swinney (2009) and Voisin, Ermanyuk & Flór (2011) for a hemispherical seamount and Shmakova, Ermanyuk & Flór (2017) for a semi-ellipsoidal seamount.

Energy radiation takes place entirely in the frequency range $|\Omega| < 1$ of propagating waves. Using (4.33), we obtain, for the cylinder,

$$\langle P \rangle = \frac{\pi}{2} \rho_{00} N (1 - \Omega^2)^{1/2} (b^2 U^2 + a^2 W^2), \tag{5.10}$$

and, for the spheroid,

$$\langle P \rangle = \frac{\pi^2}{3} \rho_{00} N a b^2 \frac{(1 - \Omega^2)^{1/2}}{(1 + |\Upsilon|^2)^{3/2}} \left[\frac{2U^2}{|1 + D(\Upsilon)|^2} + \left(\frac{1}{\Omega^2} - 1 \right) \frac{W^2}{|1 - D(\Upsilon)|^2} \right]. \tag{5.11}$$

The variations of the wave power with Ω are plotted in figure 5 for fixed excursion A and varying angle α of oscillation to the horizontal, such that $(U, W) = NA\Omega(\cos\alpha, \sin\alpha)$. The power is normalized by $P_0 = \pi \rho_{00} N^3 ab A^2$ for the cylinder and $(4/3)\pi \rho_{00} N^3 a^2 b A^2$ for the spheroid. It is a maximum at $\Omega_m = (2/3)^{1/2} \approx 0.816$ independent of α and ϵ for the cylinder, corresponding to propagation at $35°$ to the vertical, and $0.816 < \Omega_m < 1$ for the spheroid, dependent on α and ϵ, as shown in figure 6. For the sphere, Ω_m varies between 0.846 for $\alpha = 0$ and 0.835 for $\alpha = \pi/2$.

In the laboratory, when the waves are generated by an oscillating body, the excursion is usually set by practical constraints, and the frequency ratio Ω is chosen as close as possible to 0.8 in order to maximize wave radiation for that excursion, or $0.8/n$ when the generation of an nth harmonic is looked for (Shmakova *et al.* 2017). In circumstances where the waves were generated by a broadband disturbance, such as the collapse of a mixed region (Wu 1969) or a buoyant fluid parcel (Cerasoli 1978), both two-dimensional, or the decay of a three-dimensional turbulent region (Riley, Metcalfe & Weissman 1981), a well-defined peak has been observed in the wave spectrum at $\Omega_m = 0.8$, 0.7 and 0.5, respectively. If the disturbance can be viewed as an assembly of turbulent patches oscillating with random frequencies in random directions with an approximately constant excursion, then the above mechanism might explain the emergence of a well-defined peak.

6. Time-dependent aspects

At its core, added mass is a generalized susceptibility expressing the non-local temporal linear relation between a cause – the velocity $U(t)$ of the moving body – and its effect – the hydrodynamic force $F(t)$ – through the convolution integral (4.8); see Landau & Lifshitz (1980, § 123) for a presentation of generalized susceptibilities, and Landau & Lifshitz (1984, §§ 77 and 82) and Jackson (1999, § 7.10) for the particular case of the electric permittivity. We investigate the consequences of that integral in this section.

6.1. *Kramers–Kronig relations*

First comes causality, namely the fact that effect cannot precede cause. In time this means $m_{ij}(t) = 0$ for $t < 0$, and in frequency the analyticity of $m_{ij}(\omega)$ in the upper half of the complex ω plane. A variety of properties of $m_{ij}(\omega)$ follow from this, discussed by Landau & Lifshitz (1980, § 123) and Jackson (1999, § 7.10). We adapt here their conclusions to the problem at hand.

Real values of $m_{ij}(\omega)$ are obtained on the evanescent part of the real frequency axis, where $m_{ij}(\omega)$ increases from 0 to m_{ij}^∞ as ω varies from N to $+\infty$ (or $-N$ to $-\infty$), and on the positive imaginary axis, where $m_{ij}(\omega)$ increases from m_{ij}^∞ to $+\infty$ as ω varies from $i\infty$
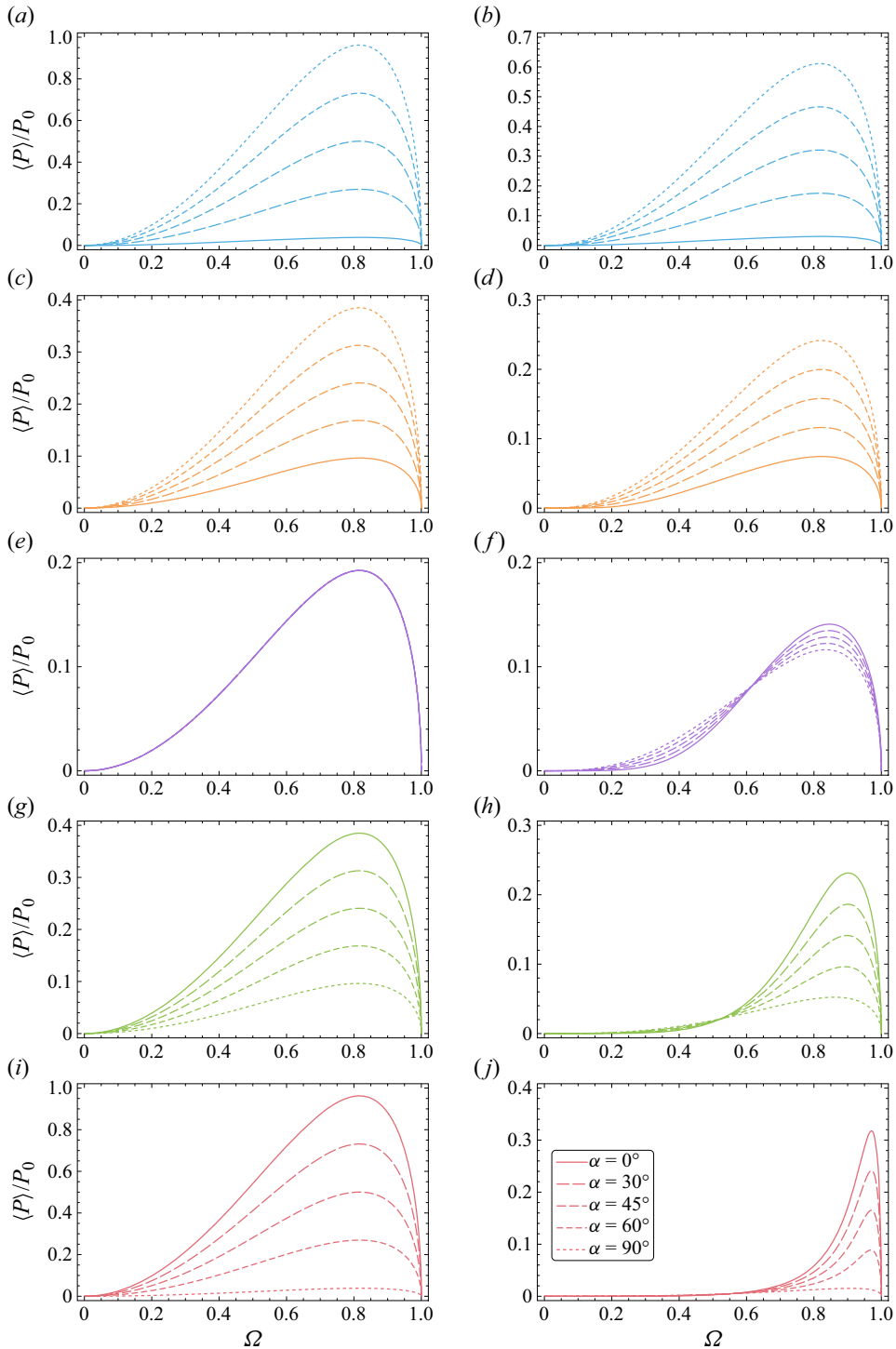
Figure 5. Frequency variations of the power outputs of (a,c,e,g,i) elliptic cylinders and (b,d,f,h,j) spheroids of aspect ratios (a,b) $\epsilon = 0.2$, (c,d) $\epsilon = 0.5$, (e,f) $\epsilon = 1$, (g,h) $\epsilon = 2$ and (i,j) $\epsilon = 5$ oscillating with fixed excursion at the angle α to the horizontal.
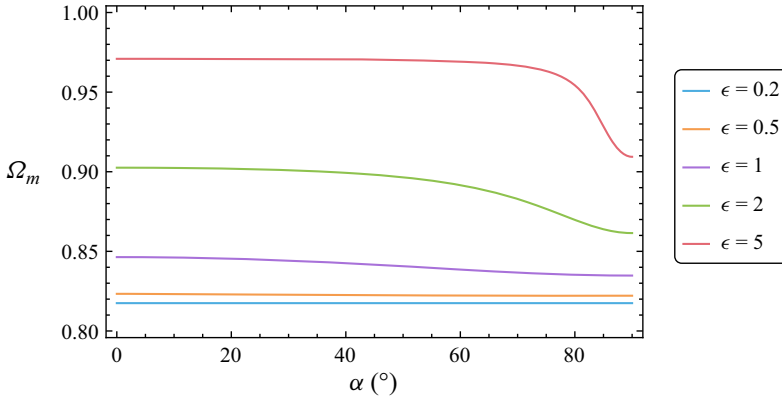
Figure 6. Frequency Ω_m of maximum power output of a spheroid of aspect ratio ϵ oscillating with fixed excursion at the angle α to the horizontal.

to i0. At infinity along any direction of the upper half-plane, we have

$$m_{ij}(\omega) = m_{ij}^{\infty} + O\left(\frac{1}{\omega^2}\right), \tag{6.1}$$

namely the oscillations are so fast that buoyancy cannot manifest itself and added mass takes its value in a homogeneous fluid. At the origin, decomposing $m_{ij}(\omega)$ into its real part $\mu_{ij}(\omega)$ and its imaginary part $\lambda_{ij}(\omega)/\omega$, we see from § 5.1 that $\lambda_{ij}(\omega)$ may be non-zero, yielding a first-order pole, and that $\mu_{ij}(\omega)$ may exhibit a logarithmic singularity.

For real ω, we integrate $[m_{ij}(\omega') - m_{ij}^{\infty}]/(\omega' - \omega)$ in the ω' plane along the contour shown in figure 7. The contribution of the large semi-circle at infinity vanishes by (6.1). The small semi-circles at the poles $\omega' = 0$ and $\omega' = \omega$ give residue contributions, to which the logarithmic divergence of $\mu_{ij}(\omega)$ at $\omega' = 0$ is too weak to contribute. We obtain

$$\pi\frac{\lambda_{ij}(0)}{\omega} + i\pi[m_{ij}(\omega) - m_{ij}^{\infty}] = \fint_{-\infty}^{\infty} \frac{m_{ij}(\omega') - m_{ij}^{\infty}}{\omega' - \omega}\, d\omega', \tag{6.2}$$

where the stroke through the integral denotes a principal value. Separating real and imaginary parts, we have

$$\mu_{ij}(\omega) - \mu_{ij}(\infty) = \frac{1}{\pi}\fint_{-N}^{N} \frac{\lambda_{ij}(\omega')}{\omega' - \omega}\frac{d\omega'}{\omega'}, \tag{6.3a}$$

$$\frac{\lambda_{ij}(\omega) - \lambda_{ij}(0)}{\omega} = -\frac{1}{\pi}\fint_{-\infty}^{\infty} \frac{\mu_{ij}(\omega') - \mu_{ij}(\infty)}{\omega' - \omega}\, d\omega', \tag{6.3b}$$

or, taking into account that $\mu_{ij}(\omega)$ and $\lambda_{ij}(\omega)$ are even functions of ω,

$$\mu_{ij}(\omega) - \mu_{ij}(\infty) = \frac{2}{\pi}\fint_{0}^{N} \frac{\lambda_{ij}(\omega')}{\omega'^2 - \omega^2}\, d\omega', \tag{6.4a}$$

$$\frac{\lambda_{ij}(\omega) - \lambda_{ij}(0)}{\omega^2} = -\frac{2}{\pi}\fint_{0}^{\infty} \frac{\mu_{ij}(\omega') - \mu_{ij}(\infty)}{\omega'^2 - \omega^2}\, d\omega'. \tag{6.4b}$$

This is the most general form of the Kramers–Kronig relations for internal waves, expressing $\mu_{ij}(\omega)$ for real frequencies in terms of $\lambda_{ij}(\omega)$ also for real frequencies, and
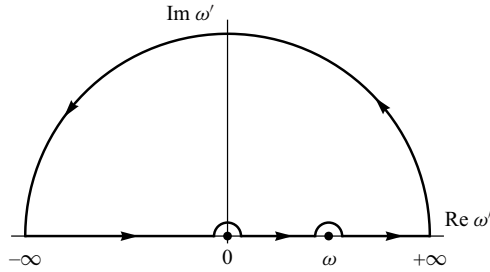
987 A27-18

Figure 7. Contour for the derivation of the Kramers–Kronig relations.

vice versa. They were verified analytically by Ermanyuk & Gavrilov (2002*a*) for a circular cylinder, using added mass coefficients deduced from Hurley (1997).

Relation (6.4*a*) may be of practical interest, as it provides a way of calculating the inertial coefficient $\mu_{ij}(\omega)$ at any real frequency, should the variations of the damping coefficient $\lambda_{ij}(\omega)$ be known exactly or determined empirically, by (4.33), from measurements of the wave power $\langle P \rangle$. Together, (6.4*a*)–(6.4*b*) may be used to deduce connections between the behaviours of the coefficients at low, intermediate and high frequencies, transferring the burden of calculating these coefficients onto the frequency range in which the calculation is easiest, as pointed out for surface gravity waves by Greenhow (1984, 1986), based on Kotik & Mangulis (1962).

6.2. *Memory effect*

Physically, added mass may be decomposed into two parts: an instantaneous response with no effect of the stratification, and a delayed response caused by internal wave radiation. We write

$$m_{ij}(t) = m_{ij}^{\infty}\delta(t) + m_{ij}^{M}(t), \tag{6.5}$$

where

$$m_{ij}^{\infty} = m_{ij}(\omega = \infty), \quad m_{ij}^{M}(t) = \frac{1}{2\pi}\int [m_{ij}(\omega) - m_{ij}^{\infty}]\exp(-\mathrm{i}\omega t)\,\mathrm{d}\omega, \tag{6.6a,b}$$

so that the hydrodynamic force (4.8) becomes

$$F_i(t) = -m_{ij}^{\infty}\frac{\mathrm{d}U_j}{\mathrm{d}t}(t) - \int_0^{\infty} m_{ij}^{M}(t')\frac{\mathrm{d}U_j}{\mathrm{d}t}(t - t')\,\mathrm{d}t'. \tag{6.7}$$

Accordingly, the effect of the stratification on added mass may be characterized as a memory effect, interpreted by Newman (2017, § 6.19), for surface gravity waves, as the feedback that the pressure fluctuations in the waves, once generated by the body, will continue to have on this body as they propagate away, for all subsequent times.

The memory kernel $m_{ij}^{M}(t)$, or impulse response function (Cummins 1962; Ogilvie 1964), may be expressed as the coefficient

$$C_{ij}^{M}(t) = \frac{m_{ij}^{M}(t)}{Nm_f} = \frac{1}{2\pi N}\int [C_{ij}(\omega) - C_{ij}^{\infty}]\exp(-\mathrm{i}\omega t)\,\mathrm{d}\omega. \tag{6.8}$$

It is a real causal function, $f(t)$ say, and as such may be written in terms of the real part of its Fourier transform $f(\omega)$ alone, or the imaginary part alone, as

$$f(t) = \frac{2}{\pi}H(t)\int_0^{\infty}\mathrm{Re}[f(\omega)]\cos(\omega t)\,\mathrm{d}\omega = \frac{2}{\pi}H(t)\int_0^{N}\mathrm{Im}[f(\omega)]\sin(\omega t)\,\mathrm{d}\omega. \tag{6.9}$$
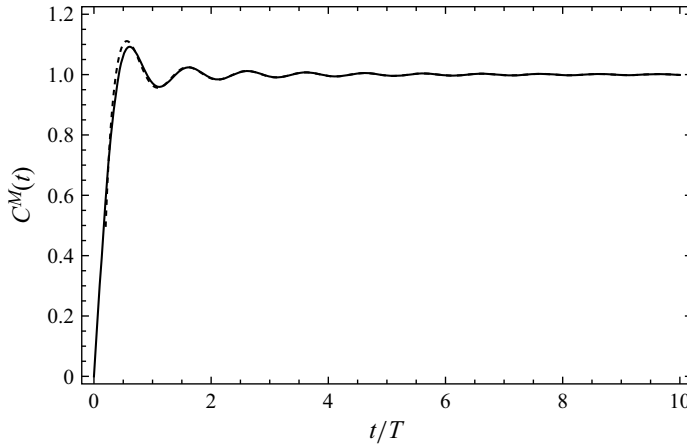
Figure 8. Exact (solid line) and asymptotic (dashed line) variations of the memory kernel for the translation of an elliptic cylinder.

Account has been taken of the fact that the imaginary part, proportional to the damping coefficient $\lambda_{ij}(\omega)$, is non-zero only over the propagating frequency range $|\omega| < N$.

Changing variable according to $\omega = N \cos \theta$, we obtain, for the elliptic cylinder,

$$C_x^M(t) = \epsilon C^M(t), \quad C_z^M(t) = \frac{1}{\epsilon} C^M(t), \tag{6.10a,b}$$

where

$$C^M(t) = \frac{2}{\pi} H(t) \int_0^{\pi/2} \sin(Nt \cos \theta) \frac{\sin^2 \theta}{\cos \theta} \, d\theta, \tag{6.11}$$

or alternatively, in terms of the Bessel functions $J_n(t)$,

$$C^M(t) = H(t) \int_0^t J_1(N\tau) \frac{d\tau}{\tau}. \tag{6.12}$$

Using (10.22.2) from Olver *et al.* (2010), we have

$$\int_0^t J_1(N\tau) \frac{d\tau}{\tau} = Nt J_0(Nt) \left[1 - \frac{\pi}{2} \boldsymbol{H}_1(Nt) \right] - J_1(Nt) \left[1 - \frac{\pi}{2} Nt \boldsymbol{H}_0(Nt) \right], \tag{6.13}$$

where $\boldsymbol{H}_n(t)$ denotes a Struve function. The variations of the kernel are the same for horizontal and vertical motions. They are plotted in figure 8 where time is normalized by the buoyancy period $T = 2\pi/N$.

Their interpretation is made easier by the expansion of the kernel for large time $Nt \gg 1$. Lighthill (1958, chapter 4) showed that the asymptotic behaviour of a Fourier transform follows from expanding the original function near the points where it, or any of its successive derivatives, is singular, then transforming these expansions and adding the results. The same applies to an inverse transform such as (6.8). The singularities are a pole at $\omega = 0$ and two branch points at $\omega = \pm N$. Their contributions are evaluated using table 4 of Voisin (2003), to give

$$C^M(t) \sim 1 - \left(\frac{2}{\pi} \right)^{1/2} \frac{\cos(Nt - \pi/4)}{(Nt)^{3/2}}. \tag{6.14}$$

This expansion, shown in figure 8, is seen to hold for almost any value of Nt. The kernel thus superposes buoyancy oscillations of frequency N and amplitude decaying as $t^{-3/2}$,

987 A27-20

faster than the decay as $t^{-1/2}$ of the kernel of the Basset–Boussinesq memory integral (Boussinesq 1885; Basset 1888), to a constant value. Accordingly, however much time has passed, the force exerted on the cylinder remains affected by the full past history of its motion. This feature is specific to two dimensions.

For the spheroid, we have

$$C_x^M(t) = 2\frac{H(t)}{\epsilon} \int_0^{\pi/2} \sin(Nt\cos\theta)\cos\theta(1 + \epsilon^2\tan^2\theta)^{3/2}$$

$$\times \left\{ \frac{\pi^2}{4} + \left[\operatorname{arcsinh}(\epsilon\tan\theta) - \frac{2 + \epsilon^2\tan^2\theta}{\epsilon\tan\theta}(1 + \epsilon^2\tan^2\theta)^{1/2} \right]^2 \right\}^{-1} \mathrm{d}\theta, \tag{6.15a}$$

$$C_z^M(t) = \frac{H(t)}{\epsilon} \int_0^{\pi/2} \sin(Nt\cos\theta)\frac{\sin^2\theta}{\cos\theta}(1 + \epsilon^2\tan^2\theta)^{3/2}$$

$$\times \left\{ \frac{\pi^2}{4} + [\operatorname{arcsinh}(\epsilon\tan\theta) + \epsilon\tan\theta(1 + \epsilon^2\tan^2\theta)^{1/2}]^2 \right\}^{-1} \mathrm{d}\theta, \tag{6.15b}$$

namely different variations for horizontal and vertical motions, which cannot be expressed in terms of known functions. They are plotted in figure 9 and take the form of decaying buoyancy oscillations at the frequency N, superposed to a monotonous decrease for vertical motion and a slow non-monotonous variation for horizontal motion.

Lighthill's (1958) asymptotic approach, used for the cylinder, considers only real values of the original and transformed variables, and hence, can only give algebraic decays with or without oscillations. These are indeed the behaviours observed for very large Nt in all circumstances, but not, for moderately large Nt, the behaviour observed in figure 9 for horizontal motion. A generalization of the approach is in order, taking complex singularities into account and evaluating their contributions as contour integrals gathered in Appendix C. The best outcome, encompassing the cylinder as a particular case, is obtained by considering the singularities at which either the modulus of the transform diverges, or a branch cut starts across which this modulus undergoes a jump.

The singularities of $C_x(\omega)$ and $C_z(\omega)$ are linked to those of $D(\Upsilon)$, whose variations are shown in figure 10. The only singularity is a branch point at $\Upsilon = -1$, with a cut along the negative real axis. In the plane of the complex variable ω, scaled as $\Omega = \omega/N$, to which Υ is related by (5.4), three or four singularities are observed depending on the parameter ϵ: two singularities at $\Omega = \pm 1$, corresponding to $\Upsilon = 0$, in the vicinity of which

$$D(\Upsilon) \sim 1 - \frac{\pi}{2}\Upsilon \sim 1 - \pi\epsilon\left[\left(\frac{\Omega - 1}{2}\right)^{1/2}, \mathrm{i}\left(\frac{\Omega + 1}{2}\right)^{1/2} \right], \tag{6.16}$$

yielding an algebraically decaying oscillation at the buoyancy frequency; one singularity at $\Omega = 0$, corresponding to $\Upsilon \to \infty$, in the vicinity of which

$$D(\Upsilon) \sim \frac{\ln\Upsilon}{\Upsilon^2} \sim \frac{\Omega^2\ln\Omega}{\epsilon^2}, \tag{6.17}$$

yielding an aperiodic algebraic decay; and when $\epsilon < 1$, a singularity at $\Omega = -\mathrm{i}\Omega_s$ with

$$\Omega_s = \frac{\epsilon}{(1 - \epsilon^2)^{1/2}}, \tag{6.18}$$
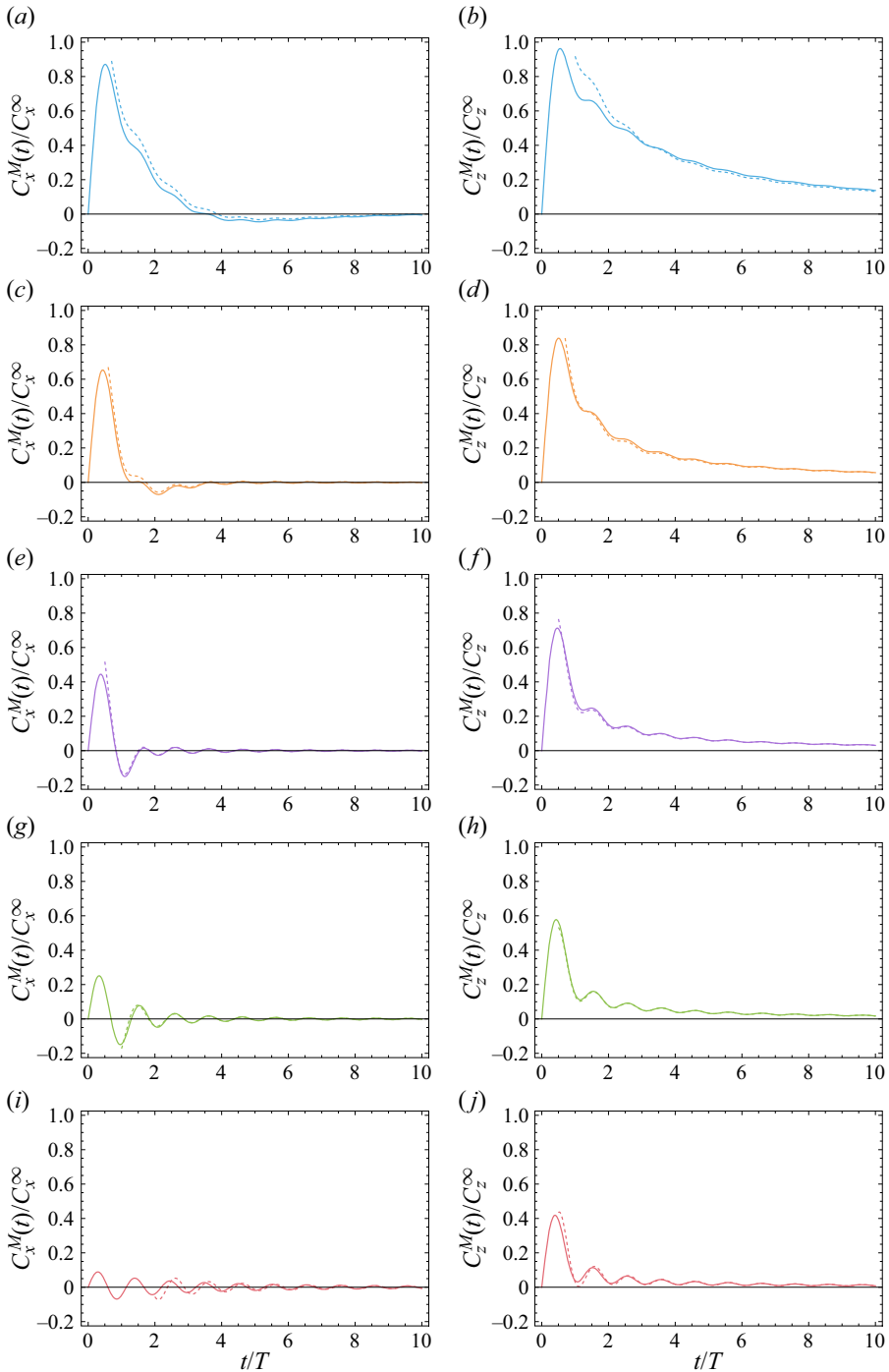
Figure 9. Exact (solid line) and asymptotic (dashed line) variations of the memory kernel for the (a,c,e,g,i) horizontal and (b,d,f,h,j) vertical translations of spheroids of aspect ratios $(a,b)\ \epsilon = 0.2$, $(c,d)\ \epsilon = 0.5$, $(e,f)\ \epsilon = 1$, $(g,h)\ \epsilon = 2$ and $(i,j)\ \epsilon = 5$.
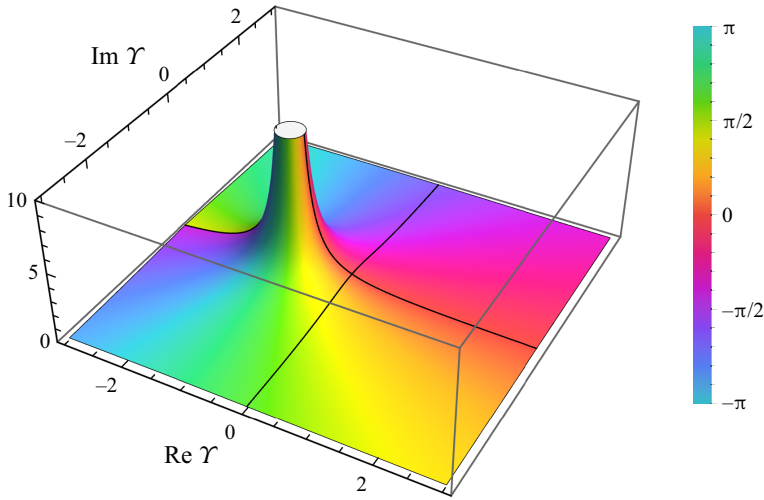
Figure 10. Variations of $D(\Upsilon)$ in the complex Υ plane. The surface height is set by the modulus of $D(\Upsilon)$ and the colour by its argument. The solid lines represent the images of the real and imaginary axes.

corresponding to $\Upsilon \rightarrow -1$, in the vicinity of which

$$D(\Upsilon) \sim \frac{\pi}{2^{3/2}(\Upsilon + 1)^{3/2}} \sim \frac{\pi}{2^{3/2}} \frac{\epsilon^{3/2}}{(1 - \epsilon^2)^{9/4}} \frac{e^{-3i\pi/4}}{(\Omega + i\Omega_s)^{3/2}}, \tag{6.19}$$

yielding an aperiodic exponential decay. The branch cut away from $\Omega = 0$ stretches along the whole negative imaginary axis when $\epsilon > 1$, and stops at $-i\Omega_s$ when $\epsilon < 1$.

Typical variations of $C_x(\omega)$ and $C_z(\omega)$ are shown in figure 11. For vertical motion, the relevant singularities are $\Omega = 0$ and $\Omega = \pm 1$. Using (C1), (C2) and (C4), we obtain

$$C_z^M(t) \sim \frac{1 - H(1 - \epsilon) \exp(-\omega_s t)}{\epsilon^2 Nt} - \left(\frac{2}{\pi}\right)^{3/2} \frac{\cos(Nt - \pi/4)}{\epsilon (Nt)^{3/2}}, \tag{6.20}$$

namely buoyancy oscillations of frequency N and amplitude decay as $t^{-3/2}$, superposed to an aperiodic decay as t^{-1}, with $\omega_s = N\Omega_s$.

For horizontal motion, the singularity $\Omega = 0$ is no longer relevant but new ones come into play, associated with the complex conjugate solutions Υ_c and $\overline{\Upsilon_c}$ of $D(\Upsilon) = -1$, where

$$\Upsilon_c \approx -1.446 + i\,0.953. \tag{6.21}$$

A new constraint arises, $|\text{Re}\ \Omega| < 1$ and $\text{Im}\ \Omega < 0$, namely the singularities must be situated in the lower half-plane between the two branch cuts away from $\Omega = \pm 1$, in order to belong to the proper Riemann sheet. This gives $\epsilon < \epsilon_c \approx 2.396$ and leaves two poles $\pm \Omega_r - i\Omega_i$, symmetric with respect to the imaginary axis, where

$$\Omega_r - i\Omega_i = \frac{\epsilon}{(\epsilon^2 - \Upsilon_c^2)^{1/2}}, \tag{6.22}$$

and the determination of the square root is chosen such that $0 < \Omega_r < 1$ and $\Omega_i > 0$. Figure 11 illustrates how the poles approach the cuts as ϵ increases, eventually crossing
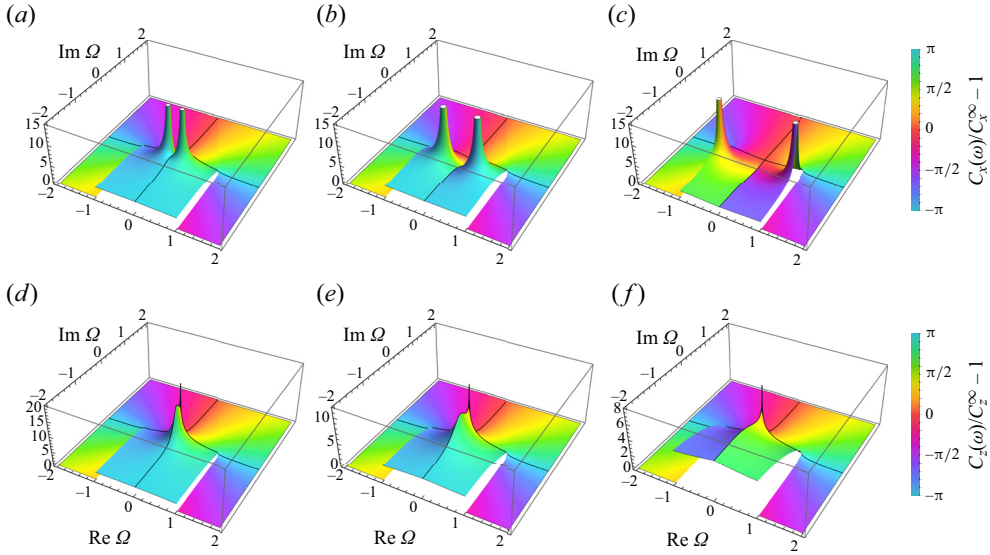
Figure 11. Variations of (*a–c*) $C_x(\omega)$ in the complex Ω plane for the horizontal translation of spheroids, and (*d–f*) $C_z(\omega)$ for their vertical translation. The spheroids have aspect ratios (*a,d*) $\epsilon = 0.5$, (*b,e*) $\epsilon = 1$ and (*c,f*) $\epsilon = 2$.

them at $\epsilon = \epsilon_c$ then vanishing. Applying the residue theorem together with (C2), we obtain

$$C_x^M(t) \sim 2\epsilon H(\epsilon_c - \epsilon) \exp(-\omega_i t) \, \mathrm{Im}\left[\frac{\Upsilon_c^2 - 1}{\Upsilon_c^2 + 1} \frac{\Upsilon_c^2 \exp(-\mathrm{i}\omega_r t)}{(\epsilon^2 - \Upsilon_c^2)^{3/2}}\right] - \epsilon \frac{\pi^{1/2}}{2^{3/2}} \frac{\cos(Nt - \pi/4)}{(Nt)^{3/2}},$$
(6.23)

namely buoyancy oscillations of frequency N and amplitude decay as $t^{-3/2}$, superposed for $\epsilon < \epsilon_c$ to oscillations of frequency $\omega_r = N\Omega_r$ and damping rate $\omega_i = N\Omega_i$.

As a rule, for both horizontal and vertical motions, the importance of the memory integral in the total hydrodynamic force (6.7) is larger for small ϵ, namely for bodies that are horizontally flat. In these circumstances, the recent history of the motion is dominant, with the memory kernel exhibiting a peak within the first half-period followed by exponential decay for horizontal motion and algebraic decay for vertical motion. As ϵ increases and the body gets more elongated vertically, the decay happens faster, hence, the peak becomes more pronounced and buoyancy oscillations take on a more prominent role afterwards. At larger ϵ the original peak remains present for vertical motion but vanishes for horizontal motion, leaving only buoyancy oscillations.

We note that $C_z^M(t)$ is always positive. Accordingly, the memory force always opposes vertical acceleration, dragging the body back as it speeds up and pushing it forward at it slows down. This is a manifestation of the inhibition of vertical motion by the stratification, complementary to the observation, both experimental and numerical, that buoyancy always induces a resistance to steady vertical motion (Magnaudet & Mercier 2020). By contrast, $C_x^M(t)$ is both positive and negative, yielding an alternation of phases where the acceleration of the body is either opposed or fostered.

987 A27-24

7. Conclusion

The concept of added mass has been generalized to stratified fluids, taking internal waves into account and assuming the fluid to be inviscid, the stratification uniform and the Boussinesq approximation valid. Added mass has been defined in § 4 for the translation of a rigid body, and its relation clarified with the hydrodynamic force on the body, the dipole strength of this body, and the energy and momentum of the fluid. Added mass has been calculated in § 5.1 for an elliptic cylinder of horizontal axis, typical of two-dimensional bodies, and a spheroid of vertical axis, typical of three-dimensional bodies, based on boundary integral representations of these bodies by Voisin (2021). Added mass appears as a complex function of the oscillation frequency ω. Its real part $\mu_{ij}(\omega)$ is associated with inertia and its imaginary part $\lambda_{ij}(\omega)/\omega$ with wave damping. The tensors $\mu_{ij}(\omega)$ and $\lambda_{ij}(\omega)$, where $i = 3$ corresponds to the vertical direction, are both symmetric; in addition, $\lambda_{ij}(\omega)$ is positive definite and vanishes outside the frequency range $|\omega| < N$ of propagating waves, with N the buoyancy frequency. Because of causality, $\mu_{ij}(\omega)$ and $\lambda_{ij}(\omega)$ satisfy Kramers–Kronig relations derived in § 6.1.

A first application of added mass is the wave power, considered in § 5.2. For the internal tide, namely internal waves generated in the ocean by the ebb and flow of the barotropic tide over bottom topography (Garrett & Kunze 2007), this power determines the rate at which barotropic energy is converted to baroclinic form. For oscillations of fixed excursion, the radiated power is a maximum at ω/N about 0.8, corresponding to radiation at $35°$ to the vertical, independent of the direction of oscillation for the cylinder and weakly dependent on it for the spheroid. This might provide an explanation for the observation, sometimes made, experimentally and numerically, of a clear peak in the wave spectrum for broadband forcing mechanisms such as the collapse of a mixed region (Wu 1969), penetrative convection (Cerasoli 1978) and turbulent decay (Riley *et al.* 1981).

Another application is the oscillations through which a buoyant body, displaced from its equilibrium position, goes back to it. These oscillations are considered in a companion paper (Voisin 2024) for three configurations: a float displaced from its neutral level then released; a Cartesian diver driven by variations of the hydrostatic pressure then released; and a pendulum with a buoyant body at its end, to which an impulse is applied. Comparison with experiment will be seen to require the inclusion of viscous dissipation.

In the temporal domain, the modifications brought to added mass by the stratification may be viewed as a new memory force, expressed in § 6.2 as a convolution integral. The kernel of this integral exhibits the same variations independent of the direction of motion for the cylinder, namely an oscillation at the buoyancy frequency with an amplitude decaying as $t^{-3/2}$, superposed to a positive constant. Accordingly, the full previous history of a two-dimensional body determines the force exerted on it at any subsequent instant. For the spheroid, the same oscillations are present, superposed to an algebraic decay as t^{-1} for vertical motion and an exponentially damped oscillation for horizontal motion. The force always opposes the acceleration of the body for vertical motion, while for horizontal motion, the acceleration is alternatively opposed and fostered.

Added mass has been investigated already for stratified fluids, in two contexts complementary to the present study. First, the inertial effect of the stratification, neglected on the Boussinesq approximation, was considered in isolation by Eames & Hunt (1997) and Palierne (1999). Second, the creeping flow regime observed in sedimentation studies, reviewed by Ardekani, Doostmohammadi & Desai (2017), Magnaudet & Mercier (2020) and More & Ardekani (2023), was considered by Candelier, Mehaddi & Vauquelin (2014) at low Reynolds and Péclet numbers, showing that stratification induces a new memory force. No detailed comparison has been attempted with the present investigation. We

note, however, that the response to the abrupt vertical motion of a sphere in figure 4 of Candelier *et al.* (2014), made of damped oscillations at the buoyancy frequency towards an equilibrium value, is similar to the response in Voisin (2024) after the abrupt release of a displaced spherical float.

An important limitation of the study is its neglect of the rotation of the body. Rotation is irrelevant – in the absence of viscosity – for the circular cylinder and the sphere for which this study was originally conceived (Voisin 2007, 2009), but it becomes essential for the elliptic cylinder and the spheroid; see the studies of settling discs by Lam, Vincent & Kanso (2019) and Mercier *et al.* (2020), and settling spheroids by More *et al.* (2021) and Varanasi, Marath & Subramanian (2022). A choice was made here to focus on translation, in order to develop the mathematical and physical tools for added mass in a stratified fluid. Given the anisotropy of the fluid, an analytical approach of rotation may prove impossible except for the simplest geometries, since all symmetries are lost when the principal axes of the body deviate from the horizontal and the vertical. In two dimensions, the small angular oscillations of an elliptic cylinder of horizontal axis and inclined cross-section were considered by Hurley & Hood (2001), theoretically, and its detailed dynamics by Hurlen (2006), theoretically, experimentally and numerically. In three dimensions, the small angular oscillations of horizontal discs were considered by Martin & Llewellyn Smith (2011, 2012).

Other limitations are the uniformity of the stratification and the unboundedness of the fluid. The studies of two-layer and composite stratifications with or without top and bottom, mentioned in § 1, show the continued relevance of added mass for these configurations, closer to coastal areas. The similarity with surface gravity waves (Wehausen 1971; Newman 1978, 2017, §§ 6.15–6.19) hints at the application of added mass to both radiation and scattering, and to the response of a body to incoming waves. The generation or scattering of an internal tide in an ocean of varying $N(z)$ and finite depth, in which the waves decompose into vertical modes, has been considered for two-dimensional topography by Pétrélis, Llewellyn Smith & Young (2006), Balmforth & Peacock (2009), Echeverri & Peacock (2010), Echeverri *et al.* (2011) and Mathur, Carter & Peacock (2014). Boundary integrals were used, and the method turned into a software package (Mercier *et al.* 2012). Given the connection of the present investigation with boundary integrals, its adaptation to more realistic configurations does not seem far away. The flexibility of the added mass concept, tied to its deeply physical nature, is illustrated by the way in which added mass has been applied, in naval hydrodynamics, to floating bodies with elastic behaviour and resonances, and to fluids with an inclined bottom or an ice cover, or with a sea state, to name but a few adaptations.

Author ORCIDs.
Ⓑ Bruno Voisin https://orcid.org/0000-0002-3741-3840.

Appendix A. Green's function

The impulsive Green's function $G(\boldsymbol{x}, t)$ represents the response to a unit point impulse. It satisfies

$$\left(\frac{\partial^2}{\partial t^2}\nabla^2 + N^2\nabla_h^2\right) G(\boldsymbol{x}, t) = \delta(\boldsymbol{x})\delta(t), \tag{A1}$$

with $\delta(\boldsymbol{x})\delta(t)$ the Dirac delta function, together with the causality condition $G|_{t<0} = 0$. It is continuous at $t = 0$ and its derivative discontinuous, with

$$G|_{t=0_+} = 0, \quad \left.\frac{\partial G}{\partial t}\right|_{t=0_+} = -\frac{1}{4\pi r}, \tag{A2a,b}$$

where $r = |\boldsymbol{x}|$. Several expressions of the Green's function may be found in the literature, namely the convolution product

$$G(\boldsymbol{x}, t) = -\frac{H(t)}{4\pi r}\int_0^t J_0\left(N\tau\frac{|z|}{r}\right) J_0[N(t-\tau)]\,d\tau, \tag{A3}$$

derived by Dickinson (1969) and Fox (1976), where $H(t)$ denotes the Heaviside step function and $J_n(t)$ a Bessel function; the spectral integral

$$G(\boldsymbol{x}, t) = -\frac{H(t)}{2\pi^2 r}\int_{N|z|/r}^N \frac{\sin(\omega t)}{(N^2 - \omega^2)^{1/2}(\omega^2 - N^2 z^2/r^2)^{1/2}}\,d\omega, \tag{A4}$$

derived by Sekerzh-Zen'kovich (1979, 1981b) and Teodorovich & Gorodtsov (1980); and the series

$$G(\boldsymbol{x}, t) = -\frac{H(t)}{2\pi N r}\sum_{n=0}^\infty J_{2n+1}(Nt)P_n\left(\frac{r_h^2 - z^2}{r^2}\right), \tag{A5}$$

derived by Gorodtsov & Teodorovich (1981) and Gordeichik & Ter-Krikorov (1996), where $\boldsymbol{x}_h = (x, y, 0)$ and $r_h = |\boldsymbol{x}_h|$, and $P_n(x)$ denotes a Legendre polynomial. The associated velocity $\boldsymbol{u}_G = [(\partial^2/\partial t^2)\nabla + N^2\nabla_h]G$ has the integral representation

$$\boldsymbol{u}_G(\boldsymbol{x}, t) = \frac{\boldsymbol{x}}{2\pi^2 r^3}\frac{\partial}{\partial t}\left\{H(t)\left[\frac{\pi}{2}\cos\left(Nt\frac{|z|}{r}\right)\right.\right.$$
$$\left.\left. + \int_{N|z|/r}^N \frac{\omega(N^2 - \omega^2)^{1/2}}{(\omega^2 - N^2 z^2/r^2)^{3/2}}\left[\cos\left(Nt\frac{|z|}{r}\right) - \cos(\omega t)\right]d\omega\right]\right\}, \tag{A6}$$

derived by Zavol'skii & Zaitsev (1984).

Another singular solution has been used by Miropol'skii (1978) and Gabov & Shevtsov (1983),

$$F(\boldsymbol{x}, t) = -\frac{H(t)}{4\pi r}\int_0^t J_0\left(N\tau\frac{|z|}{r}\right)d\tau, \tag{A7}$$

based on an analogy with the known Green's function of inertial waves (Sobolev 1954; Maslennikova 1968). It was shown by Teodorovich & Gorodtsov (1980) to satisfy

$$\left(\frac{\partial^2}{\partial t^2}\nabla^2 + N^2\nabla_h^2\right)F(\boldsymbol{x}, t) = \delta(\boldsymbol{x})\left[\delta(t) + NH(t)\int_0^t J_1(N\tau)\frac{d\tau}{\tau}\right], \tag{A8}$$

instead of (A1). The two solutions are related to each other by

$$G(\mathbf{x}, t) = \frac{\partial}{\partial t}[F(\mathbf{x}, t) * H(t)\mathrm{J}_0(Nt)], \tag{A9}$$

and their spectra by

$$\omega F(\mathbf{x}, \omega) = (\omega^2 - N^2)^{1/2} G(\mathbf{x}, \omega), \tag{A10}$$

so that

$$G(\mathbf{x}, t) = F(\mathbf{x}, t) - F(\mathbf{x}, t) * NH(t)\mathrm{J}_1(Nt), \tag{A11}$$

and conversely,

$$F(\mathbf{x}, t) = G(\mathbf{x}, t) + G(\mathbf{x}, t) * NH(t) \int_0^t \mathrm{J}_1(N\tau)\frac{\mathrm{d}\tau}{\tau}, \tag{A12}$$

as remarked by Gabov & Shevtsov (1986).

Appendix B. Kirchhoff–Helmholtz integral

The initial-boundary value problem for inertial waves was solved by Sobolev (1954) in terms of a Kirchhoff–Helmholtz integral, and the integral applied by him to initial values and by Kapitonov (1980) to boundary values. For internal waves, a Kirchhoff–Helmholtz integral was derived by Miropol'skii (1978) and Gabov & Shevtsov (1983), using $F(\mathbf{x}, t)$ as a Green's function, with Pletner (1991) adding non-Boussinesq effects and Sundukova (1991) rotation. Sekerzh-Zen'kovich (1981*a*, 1982) solved the initial-value problem in terms of the actual Green's function $G(\mathbf{x}, t)$, and Simakov (1993) introduced the use of an unspecified Green's function tailored to the Dirichlet boundary condition.

We derive the Kirchhoff–Helmholtz integral for unsteady internal waves by following the same lines as for the classical wave equation (Morse & Feshbach 1953, pp. 834–837). For arbitrary functions f and g, we write

$$f\left(\frac{\partial^2}{\partial t^2}\nabla^2 + N^2\nabla_h^2\right)g - g\left(\frac{\partial^2}{\partial t^2}\nabla^2 + N^2\nabla_h^2\right)f$$
$$= \frac{\partial}{\partial t}\left(\nabla^2 f\frac{\partial g}{\partial t} - g\frac{\partial}{\partial t}\nabla^2 f\right) - \frac{\partial}{\partial t}\boldsymbol{\nabla}\cdot\left(\boldsymbol{\nabla}f\frac{\partial g}{\partial t} - g\frac{\partial}{\partial t}\boldsymbol{\nabla}f\right)$$
$$+ \boldsymbol{\nabla}\cdot\left[f\left(\frac{\partial^2}{\partial t^2}\boldsymbol{\nabla} + N^2\boldsymbol{\nabla}_h\right)g - g\left(\frac{\partial^2}{\partial t^2}\boldsymbol{\nabla} + N^2\boldsymbol{\nabla}_h\right)f\right], \tag{B1}$$

which, integrated in time from t_1 to t_2 and in space over a volume V delimited by the surface S of outward normal $\boldsymbol{n}$, gives

$$\int_{t_1}^{t_2}\mathrm{d}t\int_V\mathrm{d}^3x\left[f\left(\frac{\partial^2}{\partial t^2}\nabla^2 + N^2\nabla_h^2\right)g - g\left(\frac{\partial^2}{\partial t^2}\nabla^2 + N^2\nabla_h^2\right)f\right]$$
$$= \int_V\mathrm{d}^3x\left[\nabla^2 f\frac{\partial g}{\partial t} - g\frac{\partial}{\partial t}\nabla^2 f\right]_{t=t_1}^{t=t_2} - \int_S\mathrm{d}^2S\left[\frac{\partial f}{\partial n}\frac{\partial g}{\partial t} - g\frac{\partial}{\partial t}\frac{\partial f}{\partial n}\right]_{t=t_1}^{t=t_2}$$
$$+ \int_{t_1}^{t_2}\mathrm{d}t\int_S\mathrm{d}^2S\left[f\left(\frac{\partial^2}{\partial t^2}\frac{\partial}{\partial n} + N^2\frac{\partial}{\partial n_h}\right)g - g\left(\frac{\partial^2}{\partial t^2}\frac{\partial}{\partial n} + N^2\frac{\partial}{\partial n_h}\right)f\right]. \tag{B2}$$

This Green's theorem is applied to wave generation by an initial disturbance at time $t = 0$ followed by boundary forcing at a closed surface S at times $t > 0$. We choose a
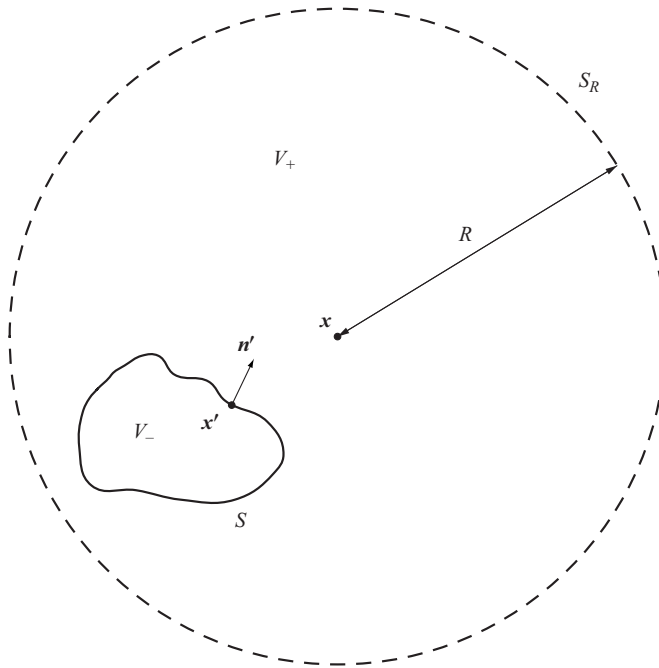
Figure 12. Geometry for the derivation of the Kirchhoff–Helmholtz integral.

fixed observation time $t > 0$, and a fixed observation point $\boldsymbol{x}$ situated either inside S in the domain V_- or outside S in the domain V_+. We integrate over t' in the interval $[0, t]$ and over $\boldsymbol{x}'$ in the domain bounded internally by S and externally by a sphere S_R of centre at $\boldsymbol{x}$ and large radius R, as shown in figure 12. We take, for f, the internal potential $\psi(\boldsymbol{x}', t')$ and, for g, the propagator $G(\boldsymbol{x} - \boldsymbol{x}', t - t')$, with G the Green's function. The contribution of S_R is assumed to vanish in the limit $R \to \infty$, an assumption we will come back to later.

We obtain

$$
\begin{aligned}
H_+(\boldsymbol{x})\psi(\boldsymbol{x}, t) = & \int_{V_+} \mathrm{d}^3 x' \left[\nabla'^2 \psi_0(\boldsymbol{x}') \frac{\partial G}{\partial t}(\boldsymbol{x} - \boldsymbol{x}', t) + \nabla'^2 \psi_1(\boldsymbol{x}') G(\boldsymbol{x} - \boldsymbol{x}', t) \right] \\
& + \int_S \mathrm{d}^2 S' \left[\frac{\partial \psi_0}{\partial n'}(\boldsymbol{x}') \frac{\partial G}{\partial t}(\boldsymbol{x} - \boldsymbol{x}', t) + \frac{\partial \psi_1}{\partial n'}(\boldsymbol{x}') G(\boldsymbol{x} - \boldsymbol{x}', t) \right] \\
& + \int_0^{t+0} \mathrm{d}t' \int_S \mathrm{d}^2 S' \left[G(\boldsymbol{x} - \boldsymbol{x}', t - t') \left(\frac{\partial^2}{\partial t'^2} \frac{\partial}{\partial n'} + N^2 \frac{\partial}{\partial n_h'} \right) \psi(\boldsymbol{x}', t') \right. \\
& \left. - \psi(\boldsymbol{x}', t') \left(\frac{\partial^2}{\partial t'^2} \frac{\partial}{\partial n'} + N^2 \frac{\partial}{\partial n_h'} \right) G(\boldsymbol{x} - \boldsymbol{x}', t - t') \right],
\end{aligned} \tag{B3}
$$

where $H_+(\boldsymbol{x}) = 1$ for $\boldsymbol{x} \in V_+$ and 0 for $\boldsymbol{x} \in V_-$ is the Heaviside step function of support V_+. The first integral on the right-hand side includes the initial disturbance

$$
\psi|_{t=0} = \psi_0(\boldsymbol{x}), \qquad \left.\frac{\partial \psi}{\partial t}\right|_{t=0} = \psi_1(\boldsymbol{x}), \tag{B4a,b}
$$

and is Sekerzh-Zen'kovich's (1981*a*, 1982) solution of the initial-value problem in the whole space. The second integral adds another initial contribution when a boundary

is present. The third integral represents the effect of the subsequent boundary forcing. It combines a single-layer potential of the general form

$$\psi_s(\boldsymbol{x}, t) = \int_0^t \mathrm{d}t' \int_S \mathrm{d}^2 S' \, \sigma(\boldsymbol{x}', t') G(\boldsymbol{x} - \boldsymbol{x}', t - t'), \tag{B5}$$

and a double-layer potential of the form

$$\psi_d(\boldsymbol{x}, t) = \int_0^{t+0} \mathrm{d}t' \int_S \mathrm{d}^2 S' \, \mu(\boldsymbol{x}', t') \left(\frac{\partial^2}{\partial t'^2} \frac{\partial}{\partial n'} + N^2 \frac{\partial}{\partial n'_h} \right) G(\boldsymbol{x} - \boldsymbol{x}', t - t'), \tag{B6}$$

with σ and μ the respective surface densities. The notation $t + 0$ means that the temporal integration ends immediately after t. If it were to end at $t - 0$, immediately before t, then an additional term would arise,

$$\int_S \mathrm{d}^2 S' \psi(\boldsymbol{x}', t) \frac{\partial}{\partial n'} \left(\frac{1}{4\pi |\boldsymbol{x} - \boldsymbol{x}'|} \right), \tag{B7}$$

associated with the delta-function singularity of $\partial^2 G/\partial t'^2 (\boldsymbol{x} - \boldsymbol{x}', t - t')$ at $t' = t$. This term may be seen in Kapitonov (1980), Gabov & Shevtsov (1983) and Simakov (1993).

The omitted contribution of S_R includes two parts. The first part,

$$- \int_{S_R} \mathrm{d}^2 S' \left[\frac{\partial \psi_0}{\partial R}(\boldsymbol{x}') \frac{\partial G}{\partial t}(\boldsymbol{x} - \boldsymbol{x}', t) + \frac{\partial \psi_1}{\partial R}(\boldsymbol{x}') G(\boldsymbol{x} - \boldsymbol{x}', t) \right], \tag{B8}$$

is associated with the initial disturbance. It vanishes as $R \to \infty$ provided that

$$\psi_0(\boldsymbol{x}') = o\left(\frac{1}{R} \right), \quad \psi_1(\boldsymbol{x}') = o\left(\frac{1}{R} \right), \tag{B9a,b}$$

which are the conditions on which Sekerzh-Zen'kovich's (1981a, 1982) solution has been obtained. The second part,

$$\int_0^{t+0} \mathrm{d}t' \int_{S_R} \mathrm{d}^2 S' \, \frac{\boldsymbol{x}' - \boldsymbol{x}}{R} \cdot [\psi(\boldsymbol{x}', t') \boldsymbol{u}_G(\boldsymbol{x}' - \boldsymbol{x}, t - t') - \boldsymbol{u}(\boldsymbol{x}', t') G(\boldsymbol{x}' - \boldsymbol{x}, t - t')], \tag{B10}$$

potentially includes waves both radiating away from the forcing and coming in from infinity. A radiation condition is needed to eliminate the latter. For steady monochromatic waves, considered in Voisin (2021), the radiation condition assumes different forms inside and outside the wave beams; this is linked to the singularity of the monochromatic Green's function along the wave rays. Here for unsteady waves, the impulsive Green's function possesses no such singularity. As $R \to \infty$, we have

$$G(\boldsymbol{x}' - \boldsymbol{x}, t - t') \sim O\left(\frac{1}{R} \right), \quad \boldsymbol{u}_G(\boldsymbol{x}' - \boldsymbol{x}, t - t') \sim O\left(\frac{1}{R^2} \right), \tag{B11a,b}$$

and the radiation condition consists in requiring that the waves decay at the same rate,

$$\psi(\boldsymbol{x}', t') \sim O\left(\frac{1}{R} \right), \quad \boldsymbol{u}(\boldsymbol{x}', t') \sim O\left(\frac{1}{R^2} \right). \tag{B12a,b}$$

With the area element $\mathrm{d}^2 S'$ varying as R^2, (B10) varies as $1/R$ and vanishes as $R \to \infty$. Sobolev (1954) noted that his (154), essentially (B2) for inertial waves, could be applied to

an unbounded domain V provided that f and g decayed at infinity as $1/R$, their first-order spatial derivatives as $1/R^2$ and the second-order derivatives as $1/R^3$.

Boundary forcing is singled out by considering motion started from rest at $t = -\infty$. We have

$$
H_+(\boldsymbol{x})\psi(\boldsymbol{x}, t) = \int_{-\infty}^{t+0} \mathrm{d}t' \int_S \mathrm{d}^2 S' \left[G(\boldsymbol{x} - \boldsymbol{x}', t - t') \left(\frac{\partial^2}{\partial t'^2} \frac{\partial}{\partial n'} + N^2 \frac{\partial}{\partial n'_h} \right) \psi(\boldsymbol{x}', t') \right.
$$
$$
\left. - \psi(\boldsymbol{x}', t') \left(\frac{\partial^2}{\partial t'^2} \frac{\partial}{\partial n'} + N^2 \frac{\partial}{\partial n'_h} \right) G(\boldsymbol{x} - \boldsymbol{x}', t - t') \right], \tag{B13}
$$

which becomes, after integrating the double-layer term twice by parts over time and using the reciprocity of the Green's function,

$$
H_+(\boldsymbol{x})\psi(\boldsymbol{x}, t) = \int_{-\infty}^{t} \mathrm{d}t' \int_S \mathrm{d}^2 S' \left[G(\boldsymbol{x} - \boldsymbol{x}', t - t') \left(\frac{\partial^2}{\partial t'^2} \frac{\partial}{\partial n'} + N^2 \frac{\partial}{\partial n'_h} \right) \psi(\boldsymbol{x}', t') \right.
$$
$$
\left. + \left(\boldsymbol{n}' \frac{\partial^2}{\partial t'^2} + \boldsymbol{n}'_h N^2 \right) \psi(\boldsymbol{x}', t') \cdot \boldsymbol{\nabla} G(\boldsymbol{x} - \boldsymbol{x}', t - t') \right]. \tag{B14}
$$

The singularity at $t' = t$ is now gone. At large distances $|\boldsymbol{x}| \gg |\boldsymbol{x}'|$ from the forcing, a multipole expansion follows from expanding the Green's function in the form

$$
G(\boldsymbol{x} - \boldsymbol{x}', t - t') \sim G(\boldsymbol{x}, t - t') - \boldsymbol{x}' \cdot \boldsymbol{\nabla} G(\boldsymbol{x}, t - t'), \tag{B15}
$$

and writing

$$
\left(\frac{\partial^2}{\partial t^2} \frac{\partial}{\partial n} + N^2 \frac{\partial}{\partial n_h} \right) \psi = u_n \quad (\boldsymbol{x} \in S), \tag{B16}
$$

with $u_n = \boldsymbol{n} \cdot \boldsymbol{u}$ the normal velocity on S. We obtain

$$
\psi(\boldsymbol{x}, t) \sim \int_{-\infty}^{t} [\mathcal{S}(t') G(\boldsymbol{x}, t - t') - \mathcal{D}(t') \cdot \boldsymbol{\nabla} G(\boldsymbol{x}, t - t')] \, \mathrm{d}t', \tag{B17}
$$

where

$$
\mathcal{S}(t) = \int_S u_n(\boldsymbol{x}, t) \, \mathrm{d}^2 S \tag{B18}
$$

is the monopole strength of the forcing and

$$
\mathcal{D}(t) = \int_S \left[\boldsymbol{x} u_n(\boldsymbol{x}, t) - \left(\boldsymbol{n} \frac{\partial^2}{\partial t^2} + \boldsymbol{n}_h N^2 \right) \psi(\boldsymbol{x}, t) \right] \mathrm{d}^2 S \tag{B19}
$$

its dipole strength.

Appendix C. Some inverse Fourier transforms

The following integrals, related to inverse Fourier transforms, are used in the present Part 1 and the companion Part 2.

First come integrals around a cut along the negative imaginary axis, shown in figure 13(a). The contour starts at infinity on the left side of the cut, encircles the branch
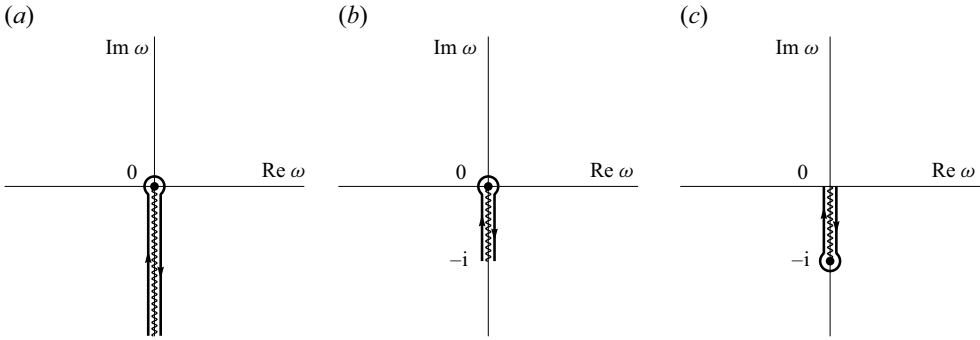
Figure 13. Integration contours for the inverse transforms in Appendix C.

point at the origin in the clockwise sense then goes back to infinity on the right-hand side. The integrals are

$$\frac{1}{2\pi} \int_{-i\infty}^{(0-)} \exp(-i\omega t)\omega^n \ln\omega \, d\omega = -\frac{n!}{i^n t^{n+1}}, \tag{C1}$$

$$\frac{1}{2\pi} \int_{-i\infty}^{(0-)} \frac{\exp(-i\omega t)}{\omega^\mu} \, d\omega = \frac{t^{\mu-1}}{\Gamma(\mu)} \exp\left(-i\mu\frac{\pi}{2}\right), \tag{C2}$$

$$\frac{1}{2\pi} \int_{-i\infty}^{(0-)} \frac{\exp(-i\omega t)}{\omega^{1/2} \pm \omega_0^{1/2}} \, d\omega = \frac{e^{-i\pi/4}}{(\pi t)^{1/2}} + i\omega_0^{1/2}\exp(-i\omega_0 t)\operatorname{erfc}[(\omega_0 t)^{1/2}e^{-i\pi/4}], \tag{C3}$$

where n is a non-negative integer, $\mu \neq -n$ a real number, $\Gamma(\mu)$ the gamma function, ω_0 a complex number such that $\operatorname{Im}[(i\omega_0)^{1/2}] > 0$ and erfc t the complementary error function.

Then come integrals along portions of that contour, namely

$$\frac{1}{2\pi} \int_{-i}^{(0-)} \exp(-i\omega t)\omega^n \ln\omega \, d\omega = -\frac{n!}{i^n t^{n+1}}\Big[1 - \exp(-t)\sum_{k=0}^{n}\frac{t^k}{k!}\Big], \tag{C4}$$

taken along the path shown in figure 13(*b*), and

$$\frac{1}{2\pi} \int_{0}^{(-i-)} \frac{\exp(-i\omega t)}{(\omega+i)^\mu} \, d\omega = -\frac{\exp(-t)}{\Gamma(\mu)}\gamma^*(1-\mu, -t)\exp\left(i\mu\frac{\pi}{2}\right), \tag{C5}$$

taken along the path shown in figure 13(*c*), with $\gamma^*(\mu, t) = t^{-\mu}\gamma(\mu, t)/\Gamma(\mu)$ a normalized form of the incomplete gamma function $\gamma(\mu, t)$.

REFERENCES

ARDEKANI, A.M., DOOSTMOHAMMADI, A. & DESAI, N. 2017 Transport of particles, drops, and small organisms in density stratified fluids. *Phys. Rev. Fluids* **2**, 100503.

BAINES, P.G. 1982 On internal tide generation models. *Deep-Sea Res.* A **29**, 307–338.

BALMFORTH, N.J. & PEACOCK, T. 2009 Tidal conversion by supercritical topography. *J. Phys. Oceanogr.* **39**, 1965–1974.

BASSET, A.B. 1888 On the motion of a sphere in a viscous liquid. *Phil. Trans. R. Soc. Lond.* A **179**, 43–63.

BATCHELOR, G.K. 1967 *An Introduction to Fluid Dynamics*. Cambridge University Press.

BOUSSINESQ, J. 1885 Sur la résistance qu'oppose un liquide indéfini en repos, sans pesanteur, au mouvement varié d'une sphère solide qu'il mouille sur toute sa surface, quand les vitesses restent bien continues et

assez faibles pour que leurs carrés et produits soient négligeables. *C. R. Hebd. Séances Acad. Sci.* **100**, 935–937.

BRENNEN, C.E. 1982 A review of added mass and fluid inertial forces. *Tech. Rep.* CR 82.010. Naval Civil Engineering Laboratory. Available at: https://resolver.caltech.edu/CaltechAUTHORS:BREncel82.

BROUZET, C., ERMANYUK, E.V., MOULIN, M., PILLET, G. & DAUXOIS, T. 2017 Added mass: a complex facet of tidal conversion at finite depth. *J. Fluid Mech.* **831**, 101–127.

BÜHLER, O. 2014 *Waves and Mean Flows*, 2nd edn. Cambridge University Press.

CADBY, J. & LINTON, C. 2000 Three-dimensional water-wave scattering in two-layer fluids. *J. Fluid Mech.* **423**, 155–173.

CANDELIER, F., MEHADDI, R. & VAUQUELIN, O. 2014 The history force on a small particle in a linearly stratified fluid. *J. Fluid Mech.* **749**, 184–200.

CERASOLI, C.P. 1978 Experiments on buoyant-parcel motion and the generation of internal gravity waves. *J. Fluid Mech.* **86**, 247–271.

CUMMINS, W.E. 1962 The impulse response function and ship motions. *Schiffstechnik* **9**, 101–109.

DAVIS, A.M.J. & LLEWELLYN SMITH, S.G. 2010 Tangential oscillations of a circular disk in a viscous stratified fluid. *J. Fluid Mech.* **656**, 342–359.

DICKINSON, R.E. 1969 Propagators of atmospheric motions. 1. Excitation by point impulses. *Rev. Geophys.* **7**, 483–514.

EAMES, I. & HUNT, J.C.R. 1997 Inviscid flow around bodies moving in weak density gradients without buoyancy effects. *J. Fluid Mech.* **353**, 331–355.

ECHEVERRI, P. & PEACOCK, T. 2010 Internal tide generation by arbitrary two-dimensional topography. *J. Fluid Mech.* **659**, 247–266.

ECHEVERRI, P., YOKOSSI, T., BALMFORTH, N.J. & PEACOCK, T. 2011 Tidally generated internal-wave attractors between double ridges. *J. Fluid Mech.* **669**, 354–374.

ERMANYUK, E.V. 2000 The use of impulse response functions for evaluation of added mass and damping coefficient of a circular cylinder oscillating in linearly stratified fluid. *Exp. Fluids* **28**, 152–159.

ERMANYUK, E.V. 2002 The rule of affine similitude for the force coefficients of a body oscillating in a uniformly stratified fluid. *Exp. Fluids* **32**, 242–251.

ERMANYUK, E.V. & GAVRILOV, N.V. 2002*a* Force on a body in a continuously stratified fluid. Part 1. Circular cylinder. *J. Fluid Mech.* **451**, 421–443.

ERMANYUK, E.V. & GAVRILOV, N.V. 2002*b* Oscillations of cylinders in a linearly stratified fluid. *J. Appl. Mech. Tech. Phys.* **43**, 503–511.

ERMANYUK, E.V. & GAVRILOV, N.V. 2003 Force on a body in a continuously stratified fluid. Part 2. Sphere. *J. Fluid Mech.* **494**, 33–50.

FERRARI, R. 2014 What goes down must come up. *Nature* **513**, 179–180.

FERRARI, R., MASHAYEK, A., MCDOUGALL, T.J., NIKURASHIN, M. & CAMPIN, J. 2016 Turning ocean mixing upside down. *J. Phys. Oceanogr.* **46**, 2239–2261.

FERRARI, R. & WUNSCH, C. 2009 Ocean circulation kinetic energy: reservoirs, sources, and sinks. *Annu. Rev. Fluid Mech.* **41**, 253–282.

FOX, D.W. 1976 Transient solutions for stratified fluid flows. *J. Res. Nat. Bur. Stand.* B **80**, 79–88.

GABOV, S.A. & SHEVTSOV, P.V. 1983 Basic boundary value problems for the equation of oscillations of a stratified fluid. *Sov. Maths Dokl.* **27**, 238–241.

GABOV, S.A. & SHEVTSOV, P.V. 1986 The method of descent and singular solutions of the equation of dynamics of a stratified liquid. *Differ. Equ.* **22**, 210–215.

GARRETT, C. & KUNZE, E. 2007 Internal tide generation in the deep ocean. *Annu. Rev. Fluid Mech.* **39**, 57–87.

GATIGNOL, R. 1983 The Faxén formulae for a rigid particle in an unsteady non-uniform Stokes flow. *J. Méc. Théor. Appl.* **2**, 143–160.

GORDEICHIK, B.N. & TER-KRIKOROV, A.M. 1996 Uniform approximations of the fundamental solution of the equation of internal waves. *J. Appl. Maths Mech.* **60**, 439–447.

GORGUI, M.A., FALTAS, M.S. & AHMED, A.Z. 1995 Motion generated by a porous wave-maker in a continuously stratified fluid. *Intl J. Engng Sci.* **33**, 757–771.

GORODTSOV, V.A. & TEODOROVICH, E.V. 1980 On the generation of internal waves in the presence of uniform straight-line motion of local and nonlocal sources. *Izv. Atmos. Ocean. Phys.* **16**, 699–704.

GORODTSOV, V.A. & TEODOROVICH, E.V. 1981 Cherenkov radiation of internal waves by a source in uniform motion. Preprint 183. Institute for Problems in Mechanics, Academy of Sciences of the USSR. In Russian.

GREENHOW, M. 1984 A note on the high-frequency limits of a floating body. *J. Ship Res.* **28**, 226–228.

GREENHOW, M. 1986 High- and low-frequency asymptotic consequences of the Kramers–Kronig relations. *J. Engng Maths* **20**, 293–306.

HURLEN, E.C. 2006 The motions and wave fields produced by an ellipse moving through a stratified fluid. PhD thesis, University of California at San Diego. Available at: https://escholarship.org/uc/item/40m4494n.

HURLEY, D.G. 1997 The generation of internal waves by vibrating elliptic cylinders. Part 1. Inviscid solution. *J. Fluid Mech.* **351**, 105–118.

HURLEY, D.G. & HOOD, M.J. 2001 The generation of internal waves by vibrating elliptic cylinders. Part 3. Angular oscillations and comparison of theory with recent experimental observations. *J. Fluid Mech.* **433**, 61–75.

JACKSON, J.D. 1999 *Classical Electrodynamics*, 3rd edn. Wiley.

KAPITONOV, B.V. 1980 Potential theory for the equation of small oscillations of a rotating fluid. *Maths USSR Sbornik.* **37**, 559–579.

KENNARD, E.H. 1967 Irrotational flow of frictionless fluids, mostly of invariable density. *Tech. Rep.* 2299. David Taylor Model Basin. Available at: https://apps.dtic.mil/sti/citations/AD0653463.

KING, B., ZHANG, H.P. & SWINNEY, H.L. 2009 Tidal flow over three-dimensional topography in a stratified fluid. *Phys. Fluids* **21**, 116601.

KOCHIN, N.E., KIBEL', I.A. & ROZE, N.V. 1964 *Theoretical Hydromechanics*. Wiley.

KOROTKIN, A.I. 2009 *Added Masses of Ship Structures*. Springer.

KOTIK, J. & MANGULIS, V. 1962 On the Kramers–Kronig relations for ship motions. *Intl Shipbuild. Prog.* **9**, 361–368.

LAI, R.Y.S. & LEE, C.-M. 1981 Added mass of a spheroid oscillating in a linearly stratified fluid. *Intl J. Engng Sci.* **19**, 1411–1420.

LAM, T., VINCENT, L. & KANSO, E. 2019 Passive flight in density-stratified fluids. *J. Fluid Mech.* **860**, 200–223.

LANDAU, L.D. & LIFSHITZ, E.M. 1980 *Statistical Physics. Part 1*, 3rd edn. Pergamon.

LANDAU, L.D. & LIFSHITZ, E.M. 1984 *Electrodynamics of Continuous Media*, 2nd edn. Pergamon.

LANDAU, L.D. & LIFSHITZ, E.M. 1987 *Fluid Mechanics*, 2nd edn. Pergamon.

LARSEN, L.H. 1969 Oscillations of a neutrally buoyant sphere in a stratified fluid. *Deep-Sea Res.* **16**, 587–603.

LAWRENCE, C.J. & WEINBAUM, S. 1986 The force on an axisymmetric body in linearized, time-dependent motion: a new memory term. *J. Fluid Mech.* **171**, 209–218.

LAWRENCE, C.J. & WEINBAUM, S. 1988 The unsteady force on a body at low Reynolds number; the axisymmetric motion of a spheroid. *J. Fluid Mech.* **189**, 463–489.

LE DIZÈS, S. & LE BARS, M. 2017 Internal shear layers from librating objects. *J. Fluid Mech.* **826**, 653–675.

LEGG, S. 2021 Mixing by oceanic lee waves. *Annu. Rev. Fluid Mech.* **53**, 173–201.

LIGHTHILL, J. 1958 *An Introduction to Fourier Analysis and Generalised Functions*. Cambridge University Press.

LIGHTHILL, J. 1978 *Waves in Fluids*. Cambridge University Press.

LIGHTHILL, J. 1986 *An Informal Introduction to Theoretical Fluid Mechanics*. Oxford University Press.

LINTON, C. & MCIVER, M. 1995 The interaction of waves with horizontal cylinders in two-layer fluids. *J. Fluid Mech.* **304**, 213–229.

LLEWELLYN SMITH, S.G. & YOUNG, W.R. 2002 Conversion of the barotropic tide. *J. Phys. Oceanogr.* **32**, 1554–1566.

MACHICOANE, N., CORTET, P.-P., VOISIN, B. & MOISY, F. 2015 Influence of the multipole order of the source on the decay of an inertial wave beam in a rotating fluid. *Phys. Fluids* **27**, 066602.

MACKINNON, J.A., *et al.* 2017 Climate process team on internal wave–driven ocean mixing. *Bull. Am. Meteorol. Soc.* **98**, 2429–2454.

MAGNAUDET, J. & EAMES, I. 2000 The motion of high-Reynolds-number bubbles in inhomogeneous flows. *Annu. Rev. Fluid Mech.* **32**, 659–708.

MAGNAUDET, J. & MERCIER, M.J. 2020 Particles, drops, and bubbles moving across sharp interfaces and stratified layers. *Annu. Rev. Fluid Mech.* **52**, 61–91.

MARTIN, P.A. & LLEWELLYN SMITH, S.G. 2011 Generation of internal gravity waves by an oscillating horizontal disc. *Proc. R. Soc. Lond.* A **467**, 3406–3423.

MARTIN, P.A. & LLEWELLYN SMITH, S.G. 2012 Generation of internal gravity waves by an oscillating horizontal elliptical plate. *SIAM J. Appl. Maths* **72**, 725–739.

MASLENNIKOVA, V.N. 1968 L_p-estimates and the asymptotic behavior as $t \rightarrow \infty$ of a solution of the Cauchy problem for a Sobolev system. *Proc. Steklov Inst. Maths* **103**, 123–150.

MATHUR, M., CARTER, G.S. & PEACOCK, T. 2014 Topographic scattering of the low-mode internal tide in the deep ocean. *J. Geophys. Res. Oceans* **119**, 2165–2182.

MAXEY, M.R. & RILEY, J.J. 1983 Equation of motion for a small rigid sphere in a nonuniform flow. *Phys. Fluids* **26**, 883–889.

MERCIER, M.J., GHAEMSAIDI, S.J., ECHEVERRI, P., MATHUR, M. & PEACOCK, T. 2012 iTides. Available at: https://doi.org/10.5281/zenodo.4421548.

MERCIER, M.J., WANG, S., PÉMÉJA, J., ERN, P. & ARDEKANI, A.M. 2020 Settling disks in a linearly stratified fluid. *J. Fluid Mech.* **885**, A2.

MILNE-THOMSON, L.M. 1968 *Theoretical Hydrodynamics*, 5th edn. Dover.

MIROPOL'SKII, Y.Z. 1978 Self-similar solutions of the Cauchy problem for internal waves in an unbounded fluid. *Izv. Atmos. Ocean. Phys.* **14**, 673–679.

MORE, R.V. & ARDEKANI, A.M. 2023 Motion in stratified fluids. *Annu. Rev. Fluid Mech.* **55**, 157–192.

MORE, R.V., ARDEKANI, M.N., BRANDT, L. & ARDEKANI, A.M. 2021 Orientation instability of settling spheroids in a linearly density-stratified fluid. *J. Fluid Mech.* **929**, A7.

MORSE, P.M. & FESHBACH, H. 1953 *Methods of Theoretical Physics. Part I.* Feshbach Publishing.

MOTYGIN, O.V. & STUROVA, I.V. 2002 Wave motions in a two-layer fluid driven by small oscillations of a cylinder intersecting the interface. *Fluid Dyn.* **37**, 600–613.

NEWMAN, J.N. 1978 The theory of ship motions. *Adv. Appl. Mech.* **18**, 221–283.

NEWMAN, J.N. 2017 *Marine Hydrodynamics*, 40th Anniv. edn. MIT Press.

OGILVIE, T.F. 1964 Recent progress toward the understanding and prediction of ship motions. In *Proceedings of the 5th Symposium on Naval Hydrodynamics* (ed. J.K. Lunde & S.W. Doroff), pp. 3–80. U.S. Government Printing Office. Available at: http://resolver.tudelft.nl/uuid:73776ccf-258f-4d5d-ab6c-88c95a002091.

OLVER, F.W.J., LOZIER, D.W., BOISVERT, R.F. & CLARK, C.W. 2010 *NIST Handbook of Mathematical Functions*. NIST/Cambridge University Press.

PALIERNE, J.F. 1999 On the motion of rigid bodies in incompressible inviscid fluids of inhomogeneous density. *J. Fluid Mech.* **393**, 89–98.

PAPOUTSELLIS, C.E., MERCIER, M.J. & GRISOUARD, N. 2023 Internal tide generation from non-uniform barotropic body forcing. *J. Fluid Mech.* **964**, A20.

PÉTRÉLIS, F., LLEWELLYN SMITH, S. & YOUNG, W.R. 2006 Tidal conversion at a submarine ridge. *J. Phys. Oceanogr.* **36**, 1053–1071.

PIERCE, A.D. 2019 *Acoustics*, 3rd edn. Springer.

PLETNER, Y.D. 1991 The fundamental solution of the equation of internal waves and some initial–boundary value problems. *Comput. Maths Math. Phys.* **31** (4), 79–88.

RILEY, J.J., METCALFE, R.W. & WEISSMAN, M.A. 1981 Direct numerical simulations of homogeneous turbulence in density-stratified fluids. *AIP Conf. Proc.* **76**, 79–112.

RODDIER, F. 1971 *Distributions et Transformation de Fourier*. McGraw-Hill.

SAFFMAN, P.G. 1992 *Vortex Dynamics*. Cambridge University Press.

SARKAR, S. & SCOTTI, A. 2017 From topographic internal gravity waves to turbulence. *Annu. Rev. Fluid Mech.* **49**, 195–220.

SEKERZH-ZEN'KOVICH, S.Y. 1979 A fundamental solution of the internal-wave operator. *Sov. Phys. Dokl.* **24**, 347–349.

SEKERZH-ZEN'KOVICH, S.Y. 1981*a* A uniqueness theorem and an explicit representation of the solution of the Cauchy problem for the equation of internal waves. *Sov. Phys. Dokl.* **26**, 21–23.

SEKERZH-ZEN'KOVICH, S.Y. 1981*b* Construction of the fundamental solution for the operator of internal waves. *J. Appl. Maths Mech.* **45**, 192–198.

SEKERZH-ZEN'KOVICH, S.Y. 1982 Cauchy problem for equations of internal waves. *J. Appl. Maths Mech.* **46**, 758–764.

SHMAKOVA, N., ERMANYUK, E. & FLÓR, J.-B. 2017 Generation of higher harmonic internal waves by oscillating spheroids. *Phys. Rev. Fluids* **2**, 114801.

SIMAKOV, S.L. 1993 Initial and boundary value problems of internal gravity waves. *J. Fluid Mech.* **248**, 55–65.

SOBOLEV, S.L. 1954 On a new problem of mathematical physics. *Izv. Akad. Nauk SSSR Ser. Mat.* **18**, 3–50. In Russian; English transl. in *Selected Works of S.L. Sobolev* (ed. G.V. Demidenko & V.L. Vaskevich), pp. 279–332. Springer (2006).

STOKES, G.G. 1851 On the effect of the internal friction of fluids on the motion of pendulums. *Trans. Camb. Phil. Soc.* **9** (2), 8–106.

STUROVA, I.V. 1994 Plane problem of hydrodynamic rocking of a body submerged in a two-layer fluid without forward speed. *Fluid Dyn.* **29**, 414–423.

STUROVA, I.V. 1999 Problems of radiation and diffraction for a circular cylinder in a stratified fluid. *Fluid Dyn.* **34**, 521–533.

STUROVA, I.V. 2001 Oscillations of a circular cylinder in a linearly stratified fluid. *Fluid Dyn.* **36**, 478–488.

STUROVA, I.V. 2003 Added masses of a cylinder intersecting the interface of a two-layer weightless fluid of finite depth. *J. Appl. Mech. Tech. Phys.* **44**, 516–521.

STUROVA, I.V. 2006 Oscillations of a cylinder piercing a linearly stratified fluid layer. *Fluid Dyn.* **41**, 619–628.

STUROVA, I.V. 2011 Hydrodynamic loads acting on an oscillating cylinder submerged in a stratified fluid with ice cover. *J. Appl. Mech. Tech. Phys.* **52**, 415–426.

STUROVA, I.V. & SYUI, C. 2005 Hydrodynamic load associated with the oscillations of a cylinder at the interface in a two-layer fluid of finite depth. *Fluid Dyn.* **40**, 273–281.

SUNDUKOVA, A.V. 1991 Fundamental solution of the gravitational–gyroscopic wave equation and the solvability of the internal and external Dirichlet problems. *Comput. Maths Math. Phys.* **31** (10), 87–93.

TEN, I. & KASHIWAGI, M. 2004 Hydrodynamics of a body floating in a two-layer fluid of finite depth. Part 1. Radiation problem. *J. Mar. Sci. Technol.* **9**, 127–141.

TEODOROVICH, E.V. & GORODTSOV, V.A. 1980 On some singular solutions of internal wave equations. *Izv. Atmos. Ocean. Phys.* **16**, 551–553.

VARANASI, A.K., MARATH, N.K. & SUBRAMANIAN, G. 2022 The rotation of a sedimenting spheroidal particle in a linearly stratified fluid. *J. Fluid Mech.* **933**, A17.

VOISIN, B. 1991 Internal wave generation in uniformly stratified fluids. Part 1. Green's function and point sources. *J. Fluid Mech.* **231**, 439–480.

VOISIN, B. 2003 Limit states of internal wave beams. *J. Fluid Mech.* **496**, 243–293.

VOISIN, B. 2007 Added mass effects on internal wave generation. In *Proceedings of the 5th International Symposium on Environmental Hydraulics* (ed. D.L. Boyer & O. Alexandrova). Available at: https://hal.archives-ouvertes.fr/hal-00268817.

VOISIN, B. 2009 Added mass in density-stratified fluids. In *Actes du 19ème Congrès Français de Mécanique* (ed. C. Rey, P. Bontoux & A. Chrisochoos). Available at: https://hal.archives-ouvertes.fr/hal-00583091.

VOISIN, B. 2021 Boundary integrals for oscillating bodies in stratified fluids. *J. Fluid Mech.* **927**, A3.

VOISIN, B. 2024 Buoyancy oscillations. *J. Fluid Mech.* **984**, A29.

VOISIN, B., ERMANYUK, E.V. & FLÓR, J.-B. 2011 Internal wave generation by oscillation of a sphere, with application to internal tides. *J. Fluid Mech.* **666**, 308–357.

WEHAUSEN, J.V. 1971 The motion of floating bodies. *Annu. Rev. Fluid Mech.* **3**, 237–268.

WHALEN, C.B., DE LAVERGNE, C., NAVEIRA GARABATO, A.C., KLYMAK, J.M., MACKINNON, J.A. & SHEEN, K.L. 2020 Internal wave-driven mixing: governing processes and consequences for climate. *Nat. Rev. Earth Environ.* **1**, 606–621.

WU, J. 1969 Mixed region collapse with internal wave generation in a density-stratified medium. *J. Fluid Mech.* **35**, 531–544.

YEUNG, R. & NGUYEN, T. 1999 Radiation and diffraction of waves in a two-layer fluid. In *Proceedings of the 22nd Symposium on Naval Hydrodynamics* (ed. Nat. Res. Counc.), pp. 875–891. National Academy Press. Available at: https://doi.org/10.17226/9771.

YOU, Y.-X., SHI, Q. & MIAO, G.-P. 2007 The radiation and diffraction of water waves by a bottom-mounted circular cylinder in a two-layer fluid. *J. Hydrodyn.* B **19**, 1–8.

ZAVOL'SKII, N.A. & ZAITSEV, A.A. 1984 Development of internal waves generated by a concentrated pulse source in an infinite uniformly stratified fluid. *J. Appl. Mech. Tech. Phys.* **25**, 862–867.

ZHANG, H.P., KING, B. & SWINNEY, H.L. 2007 Experimental study of internal gravity waves generated by supercritical topography. *Phys. Fluids* **19**, 096602.

ZHANG, W. & STONE, H.A. 1998 Oscillatory motions of circular disks and nearly spherical particles in viscous flows. *J. Fluid Mech.* **367**, 329–358.

ZILMAN, G., KAGAN, L. & MILOH, T. 1996 Hydrodynamics of a body moving over a mud layer. Part II. Added-mass and damping coefficients. *J. Ship Res.* **40**, 39–45.